RENATO BARROS ELEOTÉRIO

CARACTERIZAÇÃO DE CÉLULAS MESENQUIMAIS ESTROMAIS DA MEDULA ÓSSEA DE COELHOS ASSOCIADAS À HIDROXIAPATITA E FIBROÍNA DE SEDA NA REPARAÇÃO ÓSSEA DE COELHOS

Tese apresentada à Universidade Federal de Viçosa, como parte das exigências do Programa de Pós-Graduação em Medicina Veterinária, para obtenção do título de *Doctor Scientiae.*

VIÇOSA
MINAS GERAIS – BRASIL
2016

Ficha catalográfica preparada pela Biblioteca Central da Universidade Federal de Viçosa - Câmpus Viçosa

T
E39c
2016

Eleoterio, Renato Barros, 1985-
Caracterização de células mesenquimais estromais da medula óssea de coelhos associadas à hidroxiapatita e fibroína de seda na reparação óssea de coelhos / Renato Barros Eleoterio. – Viçosa, MG, 2016.
viii, 62f. : il. (algumas color.) ; 29 cm.

Orientador: Andréa Pacheco Batista Borges.
Tese (doutorado) - Universidade Federal de Viçosa.
Inclui bibliografia.

1. Ossos - Regeneração. 2. Materiais biomédicos. 3. Células-tronco. 4. Terapia celular. 5. Regeneração tecidual guiada. I. Universidade Federal de Viçosa. Departamento de Veterinária. Programa de Pós-graduação em Medicina Veterinária. II. Título.

CDD 22. ed. 636.089671

RENATO BARROS ELEOTÉRIO

CARACTERIZAÇÃO DE CÉLULAS MESENQUIMAIS ESTROMAIS DA MEDULA ÓSSEA DE COELHOS ASSOCIADAS À HIDROXIAPATITA E FIBROÍNA DE SEDA NA REPARAÇÃO ÓSSEA DE COELHOS

Tese apresentada à Universidade Federal de Viçosa, como parte das exigências do Programa de Pós-Graduação em Medicina Veterinária, para obtenção do título de *Doctor Scientiae.*

APROVADO: 07 de março de 2016.

Sergio Akinobu Yoshioka

Anesia Aparecida dos Santos

Emily Correna Carlo Reis
(Coorientadora)

Fabricio Luciani Valente
(Coorientador)

Andrea Pacheco Batista Borges
(Orientadora)

SUMÁRIO

LISTA DE FIGURAS

LISTA DE TABELAS

RESUMO

ELEOTÉRIO, Renato Barros, D. Sc., Universidade Federal de Viçosa, março de 2016. **Caracterização de células mesenquimais estromais da medula óssea de coelhos associadas à hidroxiapatita e fibroína de seda na reparação óssea de coelhos.** Orientadora: Andréa Pacheco Batista Borges. Coorientadores: Adriano de Paula Sabino, Emily Correna Carlo Reis e Fabricio Luciani Valente.

Terapias com células indiferenciadas são uma promissora ferramenta para aprimorar a reparação de diversos tecidos e órgãos. Muitos benefícios já foram demonstrados *in vitro*, entretanto, esforços têm sido dedicados para manter as células aplicadas *in vivo* no sítio em que se deseja a reparação, e, nesse contexto, biomateriais têm sido desenvolvidos. Assim, o objetivo do presente trabalho foi dispobilizar um método completo para obtenção, expansão e caracterização de células mesenquimais estromais (CME) oriundas da medula óssea de coelhos e avaliar o potencial de reparação óssea destas células quando utilizadas em associação com um novo biomaterial composto de hidroxiapatita e fibroína de seda (HAP/FS). Células mononucleares da medula óssea (CMMO) do úmero e fêmur de coelhos foram obtidas e, para avaliar sua taxa de proliferação, três meios de cultura diferentes foram testados. As CMMO também foram cultivadas em meios de indução osteogênico, condrogênico e adipogênico para comprovar a sua multipotencialidade. Em seguida, o biomaterial proposto foi caracterizado por difração de raios-x e microscopia eletronica de varredura, e seus efeitos na viabilidade celular e na ativação de leucócitos foram investigados. Finalmente, foi avaliada a habilidade deste biomaterial em atuar como um carreador de CME e o efeito da associação das CME ao biomaterial na reparação de defeitos ósseos na calvaria de coelhos também foi investigado. Os resultados mostraram que as técnicas aqui apresentadas fornecem um método completo para obtenção, expansão e caracterização de CME da medula óssea de coelhos de forma adequada e que a utilização destas células em associação com o compósito de HAP/SF teve um efeito benéfico na reparação dos defeitos em calvaria de coelhos.

ABSTRACT

ELEOTÉRIO, Renato Barros, D. Sc., Universidade Federal de Viçosa, March of 2016. **Characterization of mesenchymal stromal cells from rabbits' bone marrow combined to hydroxyapatite and silk fibroin in rabbits' bone repair.** Adviser: Andréa Pacheco Batista Borges. Co-advisers: Adriano de Paula Sabino, Emily Correna Carlo Reis and Fabricio Luciane Valente.

Therapies based on undifferentiated cells has been shown to be a promising tool to improve the repair of various tissues and organs. Many benefits have been demonstrated in vitro already, however, efforts have been addressed to maintain the cells applied in vivo at the site where the reparation is desired, and, in this context, biomaterials have been developed. Therefore, the aim of this study was to provide a full method to harvest, expand and characterize mesenchymal stromal cells (MSCs) from rabbits' bone marrow and to assess the bone repair potential of these cells when applied in combination to a new biomaterial composed of hydroxyapatite and silk fibroin (HAP/SF). Bone marrow mononuclear cells (BMMCs) were harvested from rabbits' humerus and femur and their proliferation rate were tested using three different culture media. BMMCs were also cultured in osteogenic, chondrogenic and adipogenic media to prove their multipotentiality. Next, the biomaterial proposed was characterized by x-ray diffraction and scanning electron microscopy, and its effects on cell viability and leukocytes activation were assessed. Finally, the biomaterial ability to act as MSCs carrier was evaluated, and its effect, in combination with the proposed biomaterial, on the repair of bone defects in rabbits' calvaria was also investigated. The results showed that the techniques presented here provide a full method for successful isolation, expansion and characterization of MSCs from rabbits' bone marrow and the utilization of these cells combined to the HAP/SF composite have had a benefic effect on the defects repair in calvaria of rabbits.

GENERAL INTRODUCTION

Undifferentiated cells, like mesenchymal stem cells, are known for being a great source for therapies based on cells, once they can differentiate into different cell lineages, like osteoblasts, chondroblasts, adipocytes and myoblasts (CAPLAN et al., 2007). Once proved their multipotentiality, mesenchymal stem cell therapy has been an important tool to improve the tissue repair and it have been used for many researchers in regenerative medicine studies.

Although there are more than 117k articles published between 1946 and January 2016 on the Nacional Center for Biotechnology Information database (NCBI) addressed to stem cell therapy, the biomedical community is still exhaustively working on this theme, aiming to establish what patients and diseases can be treated by this therapy and, importantly, assessing its long-term effects. Special attention has also been given to develop materials that can maintain stem cells at lesioned tissue sites which are aimed to be repaired. Another long list of articles focused on these materials is available on NCBI database.

The work that is presented hereafter in two chapters follows the biomedical community efforts to find a biocompatible material that can support stem cells adhesion and improve bone repair. The Biomaterials Research Group of the Veterinary Department from the Federal University of Viçosa (UFV) has extensively studied materials for bone substitution, providing publications and contributions to the bone healing, especially with use of hydroxyapatite. Over the past few years, this Biomaterials group has included stem cells in its studies and this transition motived the work described on Chapter 1. As rabbits' have some bone metabolism advantages, like a faster skeletal change and bone turnover when compared to other species (CASTAÑEDA et al. 2006), they are often used as an animal model in bone repair studies. However, when it is desired to work with undifferentiated cells of rabbits, there is few species-specific information about how to harvest and characterize this cell population. Therefore, Chapter 1 shows a full method to isolate, expand and characterize mesenchymal stromal cells from rabbits' bone marrow,

sharing the difficulties observed when cell techniques were included in the research experiments and highlighting some possible corrective actions as well.

In turn, Chapter 2 reports the combination of two different materials often used for bone repair, hydroxyapatite and silk fibroin, in a unique biomaterial with better final properties than those observed for the two materials separately. This new biomaterial was investigated by in vitro and in vivo analysis, in order to provide a new option to hold allogeneic mesenchymal stem cells within bone defects in calvaria of rabbits and improve the bone healing.

Thus, the present work provides a successful guide for mesenchymal stromal cells isolation and characterization to researches who usually work with a rabbit model, and presents a new biomaterial to be used in association with these cells to improve bone repair as well.

REFERENCES

CAPLAN, A.I. Adult mesenchymal stem cells for tissue engineering versus regenerative medicine. Journal of Cellular Physiology, v. 213, p. 341-347, 2007.

CASTAÑEDA S.; LARGO R.; CALVO E. et al. 2006. Bone mineral measurements of subchondral and trabecular bone in healthy and osteoporotic rabbits. **Skeletal Radiology**, v. 35, p. 34-41, 2006.

Chapter 1

Isolation, expansion and differentiation of mesenchymal stromal cells from rabbits' bone marrow

Renato Barros Eleotério et al.

Article accepted for publication in *Pesquisa Veterinária Brasileira*.

Isolation, expansion and differentiation of mesenchymal stromal cells from rabbits' bone marrow

ABSTRACT

Tissue engineering has been a fundamental technique in the regenerative medicine field, once it permits to build tri-dimensional tissue constructs associating undifferentiated mesenchymal cells and scaffolds in vitro. Therefore, many studies have been carried out using these cells from different animal species, and rabbits are often used as an animal model for in vivo tissue repair studies. However, most of the information available about mesenchymal stromal cells (MSCs) harvesting and characterization is about human and murine cells, which brings some doubts to the researches who desire to work with a rabbit model in tissue repair studies based on MSCs. In this context, this study aimed to add and improve the information available in the scientific literature providing a complete technique for isolation, expansion and differentiation of MSCs from rabbits. Bone marrow mononuclear cells (BMMCs) from humerus and femur of rabbits were obtained and, to evaluate their proliferation rate, three different culture media were tested, here referred as DMEM-P, DMEM´S and α-MEM. The BMMCs were also cultured in osteogenic, chondrogenic, and adipogenic induction media to prove their multipotentiality. It was concluded that the techniques suggested in this study can provide a guideline to harvest and isolate MSCs from bone marrow of rabbits in enough amount to allow their expansion. Thus, based on the laboratory experience where the study was developed, it is also suggested a culture media formulation to provide a better MSCs proliferation rate with multipotentiality preservation.

Key words: stem cells, cell therapy, tissue engineering, regenerative medicine.

INTRODUCTION

Tissue engineering has emerged as a promising alternative therapy for clinical use, once it can provide a controllable system for cell function, biological development and pathogenesis studies (GRIFFITH & NAUGHTON, 2002). Because of their ability in differentiating into a variety of cell types and relative ease of harvesting, isolation and expansion, undifferentiated stromal cells (or mesenchymal stromal cells – MSCs) have become an attractive cell population to use in tissue engineering (DAWSON et al., 2008). Thus, these cells are often associated to different biomaterials in several studies, providing tissue engineering techniques to improve the tissue regeneration process (KOTOBUKI et al., 2005).

At the same time, regenerative medicine community recognizes the need to create a database of techniques that apply undifferentiated stromal cells for clinical purpose. As rabbits have a faster skeletal change and bone turnover when compared to other species (CASTAÑEDA et al., 2006), they are usually the first choice of researchers as an animal model to assess the in vivo bone repair (LI et al., 2015). Although there are some studies available in the scientific scope about rabbits' MSCs utilization to repair different tissues (IM et al., 2001; MA et al., 2015; MEHRABANI et al., 2015; PELIZZO et al., 2015; SEMYARI et al., 2015), these studies usually fail at some point for not mentioning the whole method used to harvest and/or to prove that these cells are really undifferentiated stromal cells.

For multipotent mesenchymal stromal cells characterization, the International Society for Cellular Therapy (ISCT) establishes that they must have a fibroblastoid morphology, must be adherent to plastic, and their multipotentiality needs to be proved by inducing osteogenic, chondrogenic, and adipogenic differentiation; besides, presence of some cell surface markers and absence of others must be proved (DOMINICI et al., 2006). However, a study published by Lee et al. (2014) showed that there is not a stablished consensus about the presence of specific surface markers for rabbits' undifferentiated stromal cells as it is already consolidated for human and murine cells. In addition, these same authors suggested that those surface markers are different between the species; for example, surface markers

CD73, CD90 and CD105 are often used to identify human undifferentiated mesenchymal stem cells that are not expressed on similar cells from rabbits. Thus, this study proved that it is not accurate to introduce surface markers of human undifferentiated stromal cells to characterize those cells isolated from other species.

Therefore, the lack of information about harvesting and characterization of rabbits' MSCs can make difficult to reproduce some studies and, in some cases, this issue also brings doubts about whether these studies are really using undifferentiated stromal cells.

In this context, a complete method was elaborated to isolate, characterize, and differentiate primary mononuclear cells (BMMCs) from rabbits' bone marrow. Adapting some methods already established by other researchers and using as criteria the presence of fibroblastoid plastic-adherent cells and their ability to differentiate into the three cell lineages established by ISCT, the aim of this study was to make available a guide of techniques for researches that usually work with MSCs from a rabbit model in their tissue engineering and regenerative medicine experiments.

MATERIAL AND METHODS

Ethics statement

All the following experiments were performed at the Federal University of Viçosa (UFV)/MG, Brazil, and they were approved by the Ethics Committee on Animal Use of UFV (CEUA/UFV), as certified in the Case No. 52/2013. Rules for use of animals in research were strictly followed.

Isolation and culture of the bone marrow mononuclear cells (BMMCs)

After premedication with tramadol hydrochloride (6 mg/kg/IM), general anesthesia was induced with Tiletamine/zolazepam (30 mg/kg/IM) and maintained with isoflurane diluted in 100% oxygen by anesthesia mask. Then, surgical field was properly prepared and marrow from femur and humerus of six-month aged New Zealand rabbits was harvested. Using protocols of Tognoli et al. (2009) and Eurides et al. (2010) as reference, the bone marrow was obtained in aseptic conditions by percutaneous puncture with a hypodermic 18 G needle in rotational movements. Next, aspiration was made using a 10 ml syringe containing heparin diluted in 2 ml of sterile phosphate buffered saline (PBS) at a concentration of 5000 U/ml. In the femur, puncture was done in the region of trochanteric fossa and, in the humerus a needle was inserted into humerus tuberosity; in both cases, distal portion of the limb was pulled caudally.

Bone marrow of all limbs were extracted in the maximum amount possible. During aspiration, the syringe was carefully moved to promote homogenization between heparin and aspirated. When the aspirated marrow volume exceeded 2 ml in each member, heparin was added in an amount required to maintain the rate of 0.1 ml heparin for each 2 ml of bone marrow. After aspiration, samples were transported immediately to the cell culture laboratory in an insulated box containing ice. Donor animals were daily evaluated for one month in order to identify possible abnormalities related to bone marrow aspiration.

Meloxicam was administered at a dosage of 0.2 mg/kg subcutaneously immediately after the puncture, and then one more dosage was performed daily for 3 days.

Under class II laminar flow cabinet, the total marrow aspirated of each limb was filtered separately, to avoid contamination between samples, by 100 μM cells-strainers coupled to a 50 ml tapered bottom tube (Fig. 1A), in order to remove bone fragments and fat content.

To perform the initial counting of mononuclear cells, 0.5 ml was taken from the filtrated and mixed with 4.5 ml of 10% ammonium chloride solution, with subsequent

incubation at 4 °C for 10 minutes to cause lysis of red blood cells. Next, the solution was centrifuged at 1500 rpm for five minutes, the supernatant was discarded and the pellet was suspended in 1 ml of PBS. A 50 µl aliquot of the resuspended was mixed with 50 µl of 0.4% Trypan Blue for manual counting using a Neubauer chamber and inverted light microscopy. The remaining solution that received ammonium chloride was discarded and the filtrated remainder was transferred (Fig. 1B) to T75 culture flasks containing the culture media (Fig. 1C).

To determine an optimum culture media, which could provide better cell adaptation, cells were isolated in three different media and then a cell proliferation assay was performed for each media, which is described in the next section. The amount of media added was determined subtracting the minimum volume indicated for T75 flask (8 ml) by the volume obtained after filtration, and it was adopted no more than 4 ml of filtrate per flask. To ensure mononuclear cell adhesion, flaks were stored for three days in incubator (37° C and 5% CO_2) without media changing. After these first three days of incubation, culture media was replaced without prior washing with PBS. Further media changes were made every two or three days with carefully washing with PBS prior to addition of fresh media. When small cell clusters were observed around the flask, a first trypsinization with 4 ml of 0.25% trypsin-EDTA[1] solution diluted in PBS was performed in order to promote a better cell distribution on flask surface and thus improving intercellular interactions.

Passages were done always when cell confluence of approximately 80-90% was reached and cells were replaced in T75 culture flasks respecting the density of 4.000 cells/cm^2.

BMMCs proliferation

In order to determine an optimum culture media for the BMMCs adaptation, a proliferation assay was carried out in triplicate for three different culture media. A media often referred in the scientific literature, here called pure DMEM (DMEM-P),

[1]D59417C, Sigma-Aldrich, USA.

which consisted of 85% low glucose DMEM[2], 5% common fetal bovine serum[3] (FBS) and 10% antibiotic/antimycotic solution (0.1 g of penicillin A[4], 1 ml of gentamicin[5] at 50 µg/ml and 0.3 ml of anfotericin B[6] at 1 mg/ml for 100 ml of PBS), and two other combinations of culture media were tested. The second media was called α-MEM and consisted of 85% alpha-MEM medium[7], 10% solution antibiotics/antimycotics, 15% Qualified Fetal Bovine Serum®[8], 0.4% L-glutamine[9], and 0.4% non-essential amino acids solution[10]. The last media tested was called DMEM'S and consisted of 37.1% DMEM Advanced®[11] and 37.1% DMEM without glucose[12], with supplementation identical to that specified for the second media.

For the BMMCs proliferation analysis, 4 x 10^4 cells at the second passage were incubated in three wells of a 6 well plate. In total, 10 plates were used for each media tested. The plates were maintained in the incubator and had their media changed every two days. Every 24 hours, one plate of each media was trypsinized and then manual cell counting was performed

BMMCs differentiation

Primary mononuclear cells at fourth passage, cultured in DMEM´S media, were trypsinized and incubated in triplicate under osteogenic, adipogenic and chondrogenic induction media, as established by Sarugaser et al. (2009). For each lineage, two different media were prepared, and, therefore, it was performed two differentiation tests in triplicate for each lineage. One induction media is reported below in the description of each differentiation protocol and it refers to addition of

[2]D5648, Sigma-Aldrich, USA.
[3]16000044, Gibco, USA.
[4]P3032, Sigma-Aldrich, USA.
[5]G1397, Sigma-Aldrich, USA.
[6]A9528, Sigma-Aldrich, USA.
[7]12561056, Gibco, USA.
[8]12664025, Gibco, USA.
[9]59202C, Sigma-Aldrich, USA.
[10]M7145, Sigma-Aldrich, USA.
[11]12491015, Gibco, USA.
[12]11966025, Gibco, USA.

differentiation inductor factors proposed by Sarugaser et al. (2009) for each lineage. The second media refers to addition of L-glutamine and non-essential amino acids to the media proposed by Sarugaser et al. (2009), adjusted in the same proportion as described for DMEM'S and α-MEM proliferation assays.

For the osteogenic culture, primary cells were plated with 2 ml of DMEM'S media per well. Once reached 60% of confluence, the DMEM'S media was removed and osteogenic differentiation was induced adding 2 ml of osteogenic media composed of 44% DMEM Advanced®, 44% glucose-free DMEM, 5% Qualified Fetal Bovine Serum®, 7% antibiotic/antimycotic solution, and 1% dexamethasone 10 nM[13] diluted in ethanol. On the third culture day, 20 µL (1% of the 2 ml of induction media) of 500 mM β-glycerophosphate[14] diluted in distilled water were added into each well. Then, media was refreshed every two days, and at each refreshing, 2 ml of the induction media plus 1% of ascorbic acid[15] diluted in PBS at 5 mg/ml and 1% of 500 mM β-glycerophosphate were added. After 18 culture days, wells were washed once with PBS and fixed with 4% paraformaldehyde diluted in distilled water during 20 minutes at room temperature. Next, paraformaldehyde was removed, wells were washed once with deionized water and the staining was performed with 2% Alizarin Red diluted in deionized water (pH 4.1) in 2 wells and Von Kossa solution in one well, the last staining was performed according the protocol from Bonewald et al (2003). Dye solutions were removed after their activation times (5 minutes for Alizarin Red and 20 minutes under UV radiation for Von Kossa) by successive washes with deionized water and, after drying at room temperature, the plates were observed by inverted light microscopy.

For adipogenic culture, primary cells cells were incubated in 6-well plates on the same way as described above for osteogenic differentiation, however, the induction media was composed of 44% DMEM Advanced®, 44% DMEM glucose-free, 5% Qualified Fetal Bovine Serum®, 7% antibiotic/antimycotic solution and, for each 100 ml of this mix, it was added 50 µl of 33 µM biotin[16] (16.3 mg of biotin diluted in 1 ml of distilled water and slow addition of 1 ml of NaOH), 100 µl of 1 uM

[13]D8893, Sigma-Aldrich, USA.
[14]G9891, Sigma-Aldrich, USA.
[15]A4544, Sigma-Aldrich, USA.
[16]B4639, Sigma-Aldrich, USA.

dexamethasone, 10 µl of 100 nM bovine insulin[17] (2.87 mg of insulin diluted in 0.5 ml of distilled water with slow addition of 0.5 ml of HCL), 1.7 µl of 17 µM pantothenic acid acid[18] diluted in distilled water, 100 µl of 0.2 mM isobutyl-methylxanthine[19] diluted in dimethyl sulfoxide and 10 µl of 5 µM rosiglitazone[20] diluted in dimethyl sulfoxide. After 18 days, with medium changed every two days, cells undergoing adipogenic differentiation were washed with PBS and fixed in paraformaldehyde for one hour at room temperature. Then, paraformaldehyde was removed and the wells were washed once with deionized water. Next, a 2% Oil Red O diluted in isopropyl alcohol was prepared as a stock solution, and the work solution was prepared diluting 24 ml of the stock in 16 ml of distilled water. For staining, the monolayer was covered with work solution and left for 10 minutes before being removed with successive washings with deionized water and observed by inverted light microscope.

For chondrogenic culture, 5 x 10^5 cells at fourth passage were centrifuged in 15 ml conical bottom tubes; supernatants were discarded, and, with the cells still in pellet, 0.5 ml of chondrogenic media was added. The chondrogenic induction media was composed of 45% DMEM Advanced®, 45% DMEM glucose-free, 10% antibiotic/antimycotic solution, and 250 µl of TGF-β working solution per 5 ml of medium. To prepare the stock solution, 5 g of TGF-β[21] were diluted in 100 µL of citric acid solution 10 mM (pH 3.0). Then, for the working solution, 5 µl of the TGF-β stock solution was diluted in 1250 µl of PBS containing 2 mg/ml of bovine serum albumin[22]. The pellet was maintained in incubator for 21 days with media refreshing every two or three days. After that, pellets were fixed with 4% paraformaldehyde for 20 minutes, washed 3 times with PBS and immersed in 1% Alcian Blue dye solution diluted in a 3% acetic acid (pH 2.5). After 20 minutes, dye solution was removed and the pellets were successively washed with PBS and stored in PBS until the time of embedding in paraffin for histological processing and observation by light microscopy.

[17] I5500, Sigma-Aldrich, USA.
[18] P2250, Sigma-Aldrich, USA.
[19] I5879, Sigma-Aldrich, USA.
[20] R2408, Sigma-Aldrich, USA.
[21] PHG9204, Gibco, USA.
[22] A4503, Sigma-Aldrich, USA.

RESULTS AND DISCUSSION

Isolation and culture of the BMMCs

None of the six animals showed pain, lameness, infection at the puncture site, or appetite reduction. Both femoral and humerus punctures allowed BMMCs harvesting with an enough amount of cells to provide their expansion in vitro. However, humeral puncture occurred more easily and it allowed marrow aspiration in a larger volume (6 ml on average) than femoral puncture (4 ml on average). The average of aspirated marrow in both limbs was greater than the 2 ml quoted by Planka et al. (2008) for aspiration in iliac crest and it was also greater than the 3 ml cited by Eurides et al. (2010) and Kim et al. (2012) in humerus aspiration, all in rabbits. According to Pittenger et al. (1999), undifferentiated mesenchymal cells are present in a small percentage of bone marrow (0.001-0.01% of the total mononuclear population) and, thus, collecting greater bone marrow volume could increase the probability of a successful mesenchymal stromal cells isolation and expansion. Although it was possible to observe presence of fat and clots in the marrow aspirated, even with heparin addition, the methods of harvesting and filtering can be considered effective, once the cell-strainer removed such substances properly and provided an ideal liquid solution for plating on culture dishes.

The primary manual counting showed average of 4.7×10^6 mononuclear cells per ml of aspirated bone marrow, which is higher than the average of 3.4×10^6 reported by Im et al. (2001), close to the average of 5×10^6 reported by Yanai et al. (2005) and below the average of 20×10^6 cells/ml reported by Planka et al. (2008), all references of cells isolated from bone marrow of rabbits. These differences between numbers of isolated mononuclear cells may be related to the protocol used for the harvesting and to the variation that can occur naturally between individuals of same species and under same conditions (EURIDES et al., 2010). According Yew et al. (2012), age is another factor that might influence the number of cells isolated, once

evidences have documented that human mesenchymal stromal cells decrease in accordance with the ageing, both in number and in efficiency.

As there was a large amount of red blood cells in the filtrate, it was not possible to visualize mononuclear cells attached during the early cultivation due to red cells superposition. However, after the first media refreshing, the amount of red cells in suspension was reduced and it was possible to observe fibroblastoide-shaped cells adhered to the culture flask, albeit at a low density. As media refreshing were further being done, preceded by washings with PBS, adhered cells and their confluence were clearly identified.

BMMCs proliferation

DMEM-P was the first media to be used for rabbits' BMMCs harvesting in the laboratory routine where this study was carried out; comparing the cell growing to results obtained by other researchers using a similar media, it was observed it was presenting a delay to reach the confluence and there was also a lower amount of viable cells at the passages than that referred by other researches. Based on these initial results, it was decided to perform a cell proliferation test for DMEM-P, which confirmed a low BMMCs proliferation rate in this media. The Fig. 2A shows BMMCs reaching their maximum average of proliferation on the fourth culture day with a total of 12 x 10^4 cells; on the fifth day, this average decreased extensively, and on the sixth day the count revealed a less value than the number of cells initially seeded in each well. This result suggested that this media was probably not the best one for BMMCs isolation and expansion.

In this context, the formulations of DMEM´S and α-MEM media were tested for BMMCs proliferation. Even before doing this test with cells at fourth passage, it was observed that BMMCs reached the confluence to do the first passage earlier when cultured in DMEM'S (approximately on the 15th culture day) than in α-MEM media (approximately on the 21st culture day). Then, the proliferation assay confirmed this tendency of cells growing faster in DMEM'S than in α-MEM media. Until the fifth day,

proliferation curves indicated that cells proliferated with similar number in both media, however, from the sixth day onwards, cells cultured in DMEM'S maintained their proliferation at a rate 20 to 40% higher than when cultured in α-MEM (Fig. 2B). It can also be observed that the peak of BMMCs proliferation in α-MEM occurred on the fifth culture day, with a reduction of 50% in the number of viable cells on the sixth day. Whilst, for those cells cultured in DMEM'S, it was noticed two peaks of growth, one on the seventh and another on the tenth day of culture, both of them were higher than those values corresponding to the α-MEM segment.

Comparing the data in Tab.1 and the proliferation curves obtained with DMEM-P, DMEM'S, α-MEM media (Fig. 2), it can be observed that the utilization of a more elaborated media (DMEM'S), associating L-glutamine and nonessential amino acids to a mix of specific media and BFS of superior quality, increased cell proliferation. However, it is suggested that the differences in proliferation rates can be also related to the variation of glucose concentration, once even with L-glutamine, nonessential amino acids, and qualified BFS supplementation, there was still a significant difference between DMEM´S and α-MEM proliferation curves; analyzing each media formulation, it was noticed a difference between the glucose levels.

The benefits related to the increase of glucose level in the media for mesenchymal stromal cells culture is a subject that have been treated with caution in the field of cell therapy. As it is well known, glucose is an essential source of cellular energy and it acts as an important substrate for protein and lipid synthesis (SCHEEPERS et al., 2004). Thus, cell proliferation and metabolism are also modulated by glucose, both in physiological and in pathological conditions (LI et al., 2007). However, studies have shown that high glucose concentrations can impair original cellular functions such as apoptosis, viability, and proliferation, and change the primary cells ability in forming colonies in vitro and in vivo, regardless of their origin tissue (LI et al., 2007). Besides, high glucose concentrations may also modify the gene expression and direct the differentiation of stem cells to adipogenic over chondrogenic and osteogenic lineages (KEARTS & KHAN, 2012). On the other hand, glucose depletion improves these properties due to the overall beneficial effects already described of caloric restriction for stem cells, such as delay of cell death, senescence and ageing (CHOUDHERY et al., 2012). These reports suggest that the

damage caused by glucose level deregulation may affect the properties of undifferentiated cells in a long-term and on irreversible way (BASTIANELLI et al., 2014).

Therefore, the proliferation assay results of this study have corroborated the reports above discussed regarding to glucose interference in primary mononuclear cells cultivation. For DMEM-P media production, it was used only a low glucose media (1000 mg/L) which might have not provided all the nutrients necessary for obtaining a good cell proliferation rate. For DMEM'S, besides supplementation with L-glutamine and non-essential amino acids, an equivalent mix of a high glucose media (4500 mg/L) and a no glucose media were used, resulting in a final intermediary glucose level of 2250 mg/L, which provided the best results in this assay. In turn, the α-MEM media combined the same supplementation with L-glutamine and non-essential amino acids in a low glucose media, also resulting in the final glucose concentration of 1000 mg/L and giving a better proliferation curve than DMEM-P, but lower than that provided by DMEM'S media.

BMMCs differentiation

The protocol for mesenchymal stem cells differentiation proposed by Sarugaser et al. (2009) allowed rabbits' BMMCs to differentiate into osteogenic, adipogenic and chondrogenic lineages, as suggested by ISCT to assess the multipotenciality of stem cells. Under inverted light microscopy, nodules suggesting bone formation and a positive staining for mineral deposits were identified in the osteogenic culture (Fig. 3A), which was visible macro and microscopically, both by the red color arising from Alizarin Red dye (Figs. 3B and 3C) and by the black deposits by Von Kossa staining (Figs. 3D and 3E). In the adipogenic differentiation plates, cells filled with a greasy content were identified by inverted light microscopy (Fig. 4A), which was macroscopically visible already due to presence of an oily content through culture dishes (Fig. 4B); adipogenic differentiation was microscopically confirmed with positive staining of intracellular fat content by Oil Red

O dye solution (Fig. 4C). The histological processing of pellets derived from chondrogenic differentiation to analyze by light microscopy was hampered due to their small dimensions (Fig. 4D), especially the step of embedding in paraffin; however, the procedure enabled to identify presence of cartilage matrix typically stained in blue by Alcian blue dye (Fig. 4E).

Therefore, as the tri-lineage differentiation was not hampered in presence of L-glutamine and nonessential amino acids, this study shows that the supplementation and glucose level of DMEM´S media favored MSCs proliferation maintaining their multipotentiality.

CONCLUSION

It was concluded that both humerus and femur can be considered effective for MSCs harvesting and expansion from rabbits' bone marrow and that, among the media tested, DMEM'S matched better the nutrients to provide a cell proliferation with multipotentiality preservation. Thus, researchers who usually work with a rabbit model for experiments using rabbits' mesenchymal stromal cells may be able to reproduce the techniques presented here to harvest and characterize them properly.

REFERENCES

BASTIANELLI, D.; SICILIANO, C.; ROSA, P. et al. Influence of egr-1 in cardiac tissue-derived mesenchymal stem cells in response to glucose variations. **BioMed Research International,** 2014. Available on http://www.ncbi.nlm.nih.gov/pmc/articles/PMC4054710/pdf/BMRI2014-254793.pdf. Access on 03 Oct. 2014.

BONEWALD, L.F.; HARRIS, S. E.; ROSSER, J. Von Kossa staining alone is not sufficient to confirm that mineralization in vitro represents bone formation. **Calcified Tissue International,** v. 72, p. 537-574, 2003.

CASTAÑEDA, S.; LARGO, R.; CALVO, E. et al. Bone mineral measurements of subchondral and trabecular bone in healthy and osteoporotic rabbits. **Skeletal Radiology,** v. 35, p. 34-41, 2006.

CHOUDHERY, M. S.; KHAN, M.; MAHMOOD, R. et al. Mesenchymal stem cells conditioned with glucose depletion augments their ability to repair-infarcted myocardium. **Journal of Cellular and Molecular Medicine,** v. 16, p. 2518–2529, 2012.

DAWSON, E.; MAPILI, G.; ERICKSON, K. et al. Biomaterials for stem cell differentiation. **Advanced Drug Delivery Reviews,** v. 60, p. 215–228, 2008.

DOMINICI, M.; LE BLANC, K.; MUELLER, I. et al. Minimal criteria for defining multipotent mesenchymal stromal cells. The International Society for Cellular Therapy position statement. **Cytotherapy,** v. 8, p. 315-317, 2006.

EURIDES, D.; OLIVEIRA, B. J. N. A.; SOUZA, L. A. et al. Acquirement of bone marrow mononuclear cells by puncture of the humerus tubercle of rabbits. **Ars Veterinaria.,** v. 2, p. 71-76, 2010.

GRIFFITH, L. G.; NAUGHTON, G. Tissue engineering – current challenges and expanding opportunities. **Science,** v. 295, p. 1009–1014, 2002.

IM, G. I.; KIM, D. Y.; SHIN, J. H et al. Repair of cartilage defect in the rabbit with cultured mesenchymal stem cells from bone marrow. **The Journal of Bone and Joint Surgery. British Volume,** v. 83, p. 289-294, 2001.

KEARTS, E.; KHAN, Z. A. Unique responses of stem cell-derived vascular endothelial and mesenchymal cells to high levels of glucose. **PLoS One,** v. 7, 2012. Available on http://www.ncbi.nlm.nih.gov/pmc/articles/PMC3368917/pdf/pone.0038752.pdf. Access on 03 Oct. 2014.

KIM, S. S.; KANG, M. N.; LEE, K. Y.; LEE, M. J.; WANG, L.; KIM, H. J. Therapeutic effects of mesenchymal stem cells and hyaluronic acid injection on osteochondral defects in rabbits' knees. **Knee Surgery and Related Research,** v. 24, p. 164-172, 2012.

KOTOBUKI, N.; IOKU, K.; KAWAGOE, D. et al. Observation of osteogenic differentiation cascade of living mesenchymal stem cells on transparent hydroxyapatite ceramics. **Biomaterials,** v. 26, p. 779-785, 2005.

LEE, T-C.; LEE, T-H.; HUANG, Y-H. et al. Comparison of surface markers between human and rabbit mesenchymal stem cells. **PloS ONE,** v. 9, 2014. Available on http://www.ncbi.nlm.nih.gov/pmc/articles/PMC4224397/pdf/pone.0111390.pdf. Access on 03 Dec. 2015.

LI, Y.; CHEN, S-K.; LI, L. et al. Bone defect animal models for testing efficacy of bone substitute biomaterials. **The Journal of Othopaedic Translation,** v. 3, p. 95-104.

LI, Y-M.; SCHILLING, T.; BENISCH, P. et al. Effects of high glucose on mesenchymal stem cell proliferation and differentiation. **Biochemical and Biophysical Research Communications,** v. 363, p. 209–215, 2007.

MA, X.; SUN, Y.; CHENG, X. et al. Repair of osteochondral defects by mosaicplasty and allogeneic BMSCs transplantation. **International Journal of Clinical and Experimental Medicine,** v. 8, p. 6053-6059, 2015.

MEHRABANI, D.; BABAZADEH, M.; TANIDEH, N. et al. The healing effect of adipose-derived mesenchymal stem cells in full-thickness femoral articular cartilage defects of rabbit. **International Journal of Organ Transplantation Medicine,** v. 6, p. 165-175, 2015.

PELIZZO, G.; AVANZINI, M. A.; CORNAGLIA, A. I. et al. Mesenchymal stromal cells for cutaneous wound healing in a rabbit model: pre-clinical study applicable in the pediatric surgical setting. **Journal of Translational Medicine,** v. 13, 2015. Available on http://www.ncbi.nlm.nih.gov/pmc/articles/PMC4495634/. Access on 03 Dec. 2015.

PITTENGER, M. F.; MACKAY, A. M.; BECK, S. C. et al. Multilineage potential of adult human mesenchymal stem cells. **Science,** v. 284, p. 143-147, 1999.

PLANKA, L.; GAL, P.; KECOVA, H. et al. Allogeneic and autogenous transplantations of MSCs in treatment of the physeal bone bridge in rabbits. **BioMed Central Biotechnology,** v. 8, 2008. Available on http://www.biomedcentral.com/1472-6750/8/70. Access on 16 Sept. 2014.

SARUGASER, R.; ENNIS, J.; STANFORD, W. L. et al. Isolation, propagation, and characterization of human umbilical cord perivascular cells (HUCPVCs). **Methods in Molecular Biology,** v. 482, p. 269-279, 2009.

SCHEEPERS, A.; JOOST, H. G.; SCHÜRMANN, A. The glucose transporter families SGLT and GLUT: molecular basis of normal and aberrant function. **Journal of Parenteral and Enteral Nutrition,** v. 28, p. 364–37, 2004.

SEMYARI, H.; RAJIPOUR, M.; SABETKISH, S. et al. Evaluating the bone regeneration in calvarial defect using osteoblasts differentiated from adipose-derived mesenchymal stem cells on three different scaffolds: an animal study. **Cell Tissue Bank,** 2015. Available on http://link.springer.com/article/10.1007%2Fs10561-015-9518-5. Access on 03 Dec. 2015.

TOGNOLI, G. K.; OLSSON, D. C.; MARTINS, D. B. et al. Bone marrow mononuclear cells autotransplant in experimental corneal ulcer in dogs. **Ciência Rural,** v. 39, p. 148-155, 2009.

YANAI, T.; ISHII, T.; CHANG, F. et al. Repair of large full-thickness articular cartilage defects in the rabbit: the effects of joint distraction and autologous bone marrow-derived mesenchymal cell transplantation. **Journal of Bone Joint Surgery. British Volume,** v. 87, p. 721-729, 2005.

YEW, T. L.; HUANG, T. F.; MA, H. L. et al. Scale-up of MSC under hypoxic conditions for allogeneic transplantation and enhancing bony regeneration in a rabbit calvarial defect model. **Journal of Orthopaedic Research,** v. 30, p. 1213–1220, 2012.

Figure 1. Rabbits' bone marrow aspirate being processed under class II laminar flow cabinet. A - Marrow aspirate filtering through 100 µm cell strainer (arrow) coupled to a 50 ml tapered bottom tube. B – Transference of the resulting solution to T75 culture flasks after filtration. C - T75 culture flasks containing the culture media and the bone marrow aspirate filtrated.

Table 1. Number of BMMCs from rabbits' bone marrow at second passage (means) cultured between 1 and 10 days in DMEM-P, α-MEM and DMEM'S media, n=3

Culture days	DMEM-P	α-MEM	DMEM'S
1	500000.0	56666.7	50000.0
2	106666.7	90000.0	213333.0
3	120000.0	260000.0	230000.0
4	120000.0	346666.7	336666.7
5	50000.0	823333.3	766669.7
6	40000.0	433333.3	1006667.0
7	----------	493333.3	1153333.0
8	----------	460000.0	1006667.0
9	----------	113333.3	960000.0
10	----------	333333.3	1190000.0
Standard deviation	34889.6	219287.0	41439.7

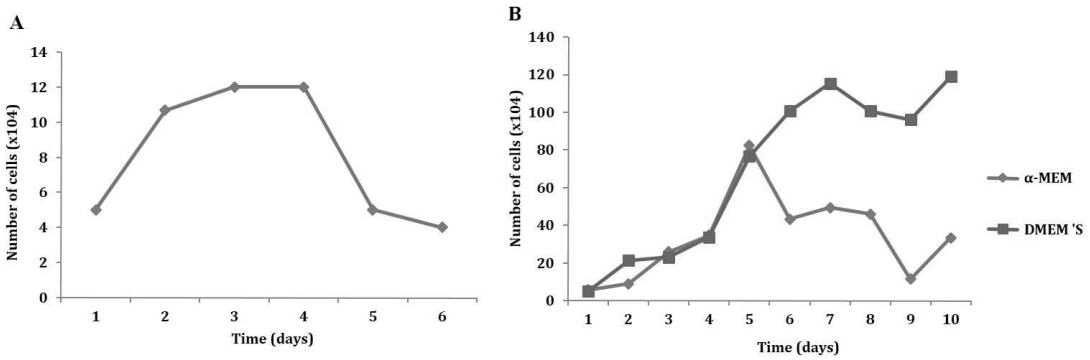

Figure 2. Proliferation curves of BMMCs from rabbits at second passage cultured in DMEM-P (A), DMEM'S (B) and α-MEM media (B), indicating that the cells have adapted and proliferated better when cultured in DMEM'S media. Lines represent a mean value, n=3/media.

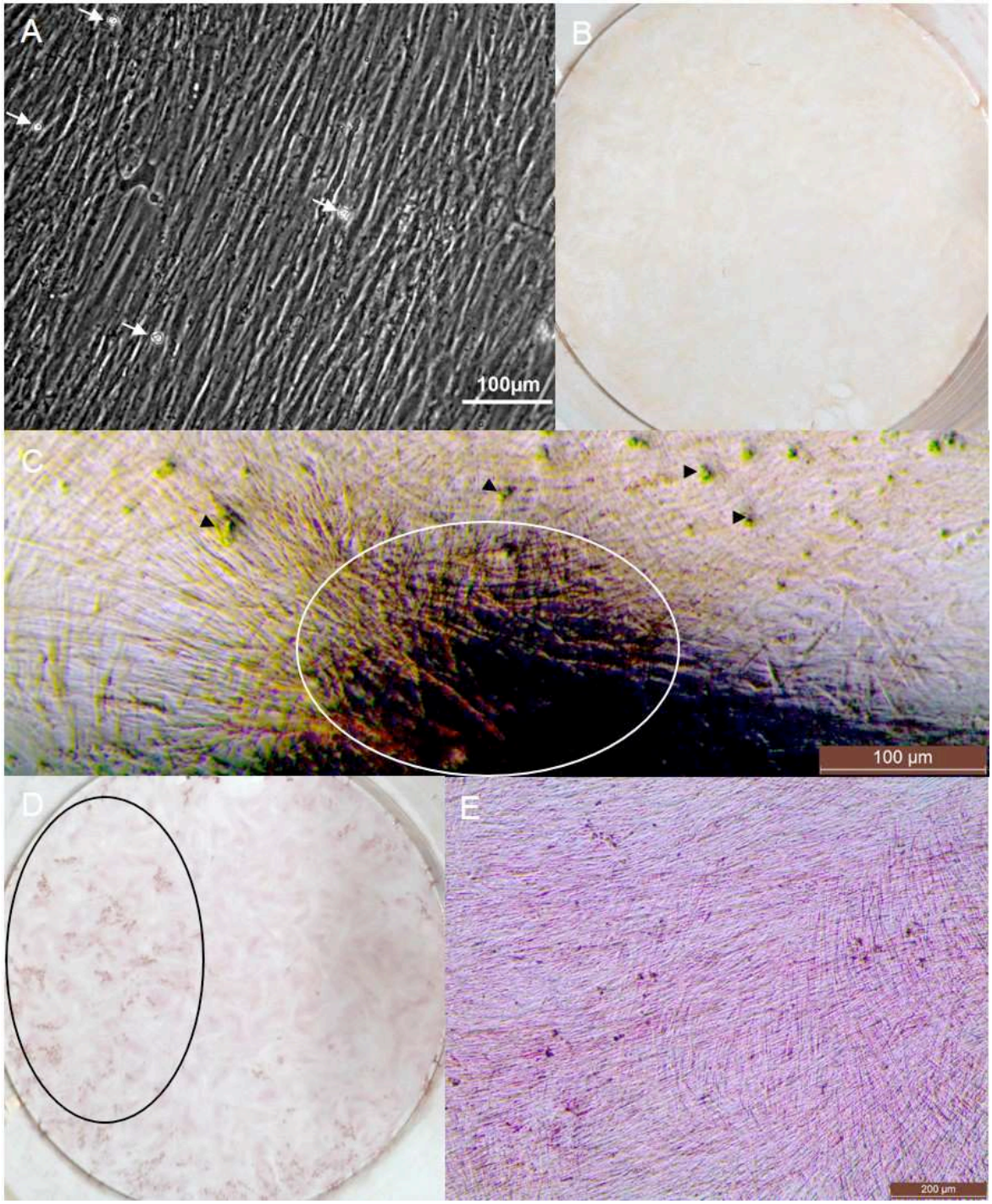

Figure 3. Images of the BMMCs culture after 18 days under osteogenic differentiation induction. A - Direct observation of the culture plate by inverted light microscope without staining. Note the presence of nodule formation (arrows) on the cell monolayer surface suggesting bone formation. B - Macroscopic view after staining with Alizarin Red. C - Image by inverted light microscopy showing presence of bone nodules formation (arrowheads) with Alizarin Red impregnation at the edges of culture dish (circled area). D - Macroscopic view of culture stained with Von Kossa, demonstrating the presence of mineral deposits stained in black distributed around the plate (circle). E - Image by inverted light microscopy confirming the presence of dots stained in black by Von Kossa distributed around the plate suggesting the presence of mineral content.

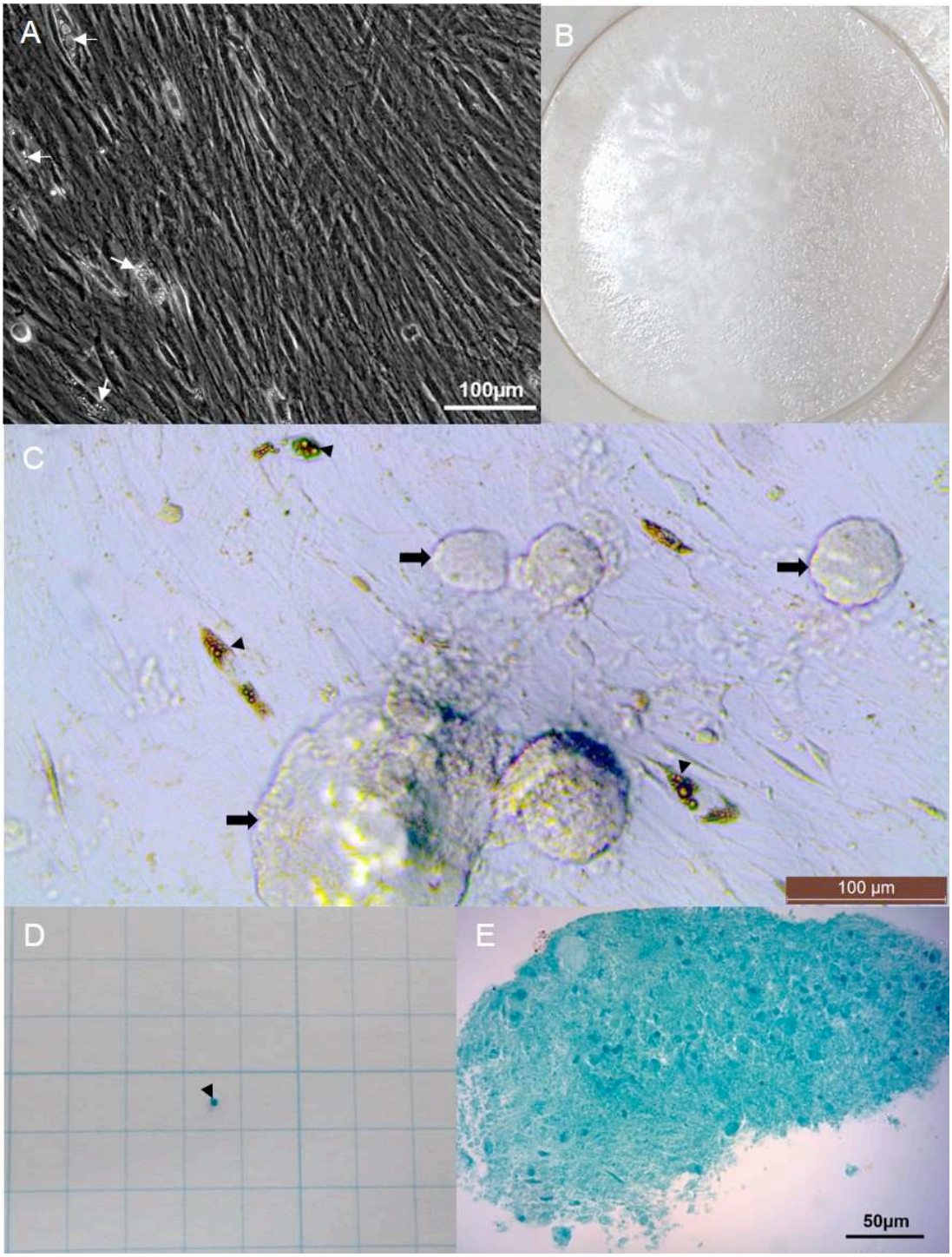

Figure 4. Images of the BMMCs culture after 18 days under adipogenic differentiation and 21 days under chondrogenic differentiation. A - Direct observation of adipogenic culture by inverted light microscope without staining. Note the presence of intracellular vesicles filled with greasy content (arrows). B – Macroscopic view of the adipogenic culture after staining with Oil Red O, indicating the presence of oily content distributed throughout the dish. C - Image by inverted light microscopy confirming the presence of fat content stained by Oil Red O, which was visible within intracellular vesicles (arrowheads) and in the extracellular environment (arrows). D - Small pellet formed after 21 days of chondrogenic culture stained with Alcian Blue (arrowhead) on 5 mm^2 squares paper. E - Histological section of the pellet observed by light microscopy, showing matrix with cartilaginous aspect, typically stained by Alcian Blue.

Chapter 2

Allogenic mesenchymal stromal cells and hydroxyapatite/silk-fibroin composite to repair bone defects in calvaria of rabbits

Renato Barros Eleotério et al.

Article being prepared.

Allogenic mesenchymal stromal cells and hydroxyapatite/silk-fibroin composite to repair bone defects in calvaria of rabbits

ABSTRACT

There is an increasing need to develop new biomaterials for bone regeneration. At the same time, the Biomaterials community recognises the need to create a database or knowledge base of techniques that apply biomaterials and undifferentiated cells in clinical applications. In this context, a new HAP/SF composite was developed and characterized, and its effects on cell viability and on leukocytes activation were investigated. In addition, it was evaluated the ability of the composite as a mesenchymal stromal cells (MSCs) carrier. Finally, the effect of allogenic MSCs transplantation associated to the proposed composite on bone defects regeneration in calvaria of 26 rabbits was investigated by clinical, micro-computed tomography, histological and histomorfometrical analysis. Results showed that the composite is biocompatible, can support the MSCs anchorage for at least the first 15 hours after implantation and did not decrease the cell proliferation nor increase leukocyte activation. In addition, it could be concluded that MSCs transplanted alone can have stimulated provisory matrix formation within the bone defects, but this new bone formation might have been accelerated and improved when the HAP/SF composite was implanted combined to the MSCs.

Key words: cell therapy, bone, biomaterials, regenerative medicine, tissue engineering.

INTRODUCTION

Surgery procedures for bone repair often require a graft to substitute and restore the function of a bone lost or damaged. Grafts can be originated from

secondary anatomic regions of the patient (autograft), from a same specie donor patient (allograft), or from a different specie donor (xenograft). Autografting is still considered the most effective method for bone healing improvement, however, this kind of graft is associated to disadvantages including limited amount of tissue that can be collected, handling difficulties in the bone graft adaption to host tissue, besides pain and morbidity at the donor site. On the other hand, allografts and xenografts are associated with disease transmission risk and potential immune rejection (KHAN et al., 2008).

The limitations associated to bone transplantation have encouraged the search for alternatives methods (CORRE et al., 2015). In addition, the development of new technologies has popularized the use of less invasive treatments. Therefore, biomaterials addressed to bone substitution have been intensively studied and gradually applied in orthopedics procedures (GU et al., 2011).

Hydroxyapatite (HAP) is the major mineral component of healthy bones and teeth. Several studies have shown that even when it is used as a synthetic biomaterial, HAP can provide advantages to bone repair, such as excellent osteoconduction, biocompatibility, and bioactivity (DOROZHKIN & EPPLE, 2002). The cellular uptake of implanted synthetic HAP granules, adjacent to new bone formation, suggests that HAP osseointegration is similar to the normal process of bone resorption/apposition (BORGES et al., 2000). Our biomaterials research group has been working extensively with different formulations of HAP and the results of our studies have confirmed its advantages to bone repair (BORGES et al., 2000; FRANCO et al., 2001; VITAL et al., 2006; CARLO et al., 2009a; CARLO et al., 2009b; REIS et al., 2010; REIS et al., 2011; REIS et al., 2013). These benefits have made synthetic HAP the most common calcium phosphate-based biomaterial used to assist bone regeneration (WANG, 2003). However, HAP as a ceramic bone substitute has also some disadvantages like brittleness, stiffness (TANAKA et al., 2007), low porosity and low capacity of degradation (HAIDAR et al., 2009). These disadvantages unable the use of HAP as unique ceramic implant material in large bone defects (WANG, 2003). In turn, the silk fibroin (SF) is biocompatible, and has appropriate flexibility and mechanical stability (KIM et al., 2005a). Then, because of these beneficial properties, new HAP/SF composites have been developed in order

to overcome the disadvantages related to the use of HAP alone (KWEON et al., 2011).

Tissue engineering is another promising alternative therapy for clinical use, once it can provide a controllable system for cell function, biological development, and pathogenesis studies (GRIFFITH & NAUGHTON, 2002). Because of their ability in differentiating into a variety of cell types and relative ease in harvesting, isolation, and expansion, undifferentiated cells like mesenchymal stromal cells (MSCs) have become an attractive cell population to use in tissue engineering and regenerative medicine studies (DAWSON et al., 2008). Thus, MSCs are often associated with different scaffold biomaterials in several studies, providing techniques to improve tissue regeneration process (KOTOBUKI et al., 2005).

In this context, a new HAP/SF composite was developed and characterized in vitro and its effects on cell viability and on leukocytes activation were investigated. Finally, the ability of this new composite as a MSCs carrier and its effect, when associated with allogenic MSC, on bone regeneration of rabbits' calvaria defects were evaluated.

MATERIAL AND METHODS

Experiments involving rabbits were performed at the Federal University of Viçosa (UFV, Brazil) with approval of the Ethics Committee on Animal Use of the UFV (CEUA/UFV), as certified in Case No. 52/2013. The rules for animals use in research were strictly followed. Experiments with human samples were performed at the University of Liverpool (U.K.), and the samples were taken after informed consent in accordance with U.K. Government regulations and with Research Ethics approval.

MSCs culture

Primary bone marrow mononuclear cells were harvested and characterized as MSCs following the procedures previously described here in Chapter 1 for MSCs isolation, expansion and differentiation. Briefly, bone marrow from humerus and femur of New Zealand rabbits approximately six-month aged was aspirated by percutaneous puncture under general anesthesia, with a hypodermic 18 G needle in rotational movements coupled to a 10 ml syringe containing heparin diluted in 2 ml of sterile phosphate buffered saline solution (PBS) at concentration of 5000 U/ml. Under class II laminar flow cabinet, the total aspirated of each limb was filtered by 100 μM cells-strainers and then plated in T75 culture flasks containing the culture media, which was composed of 37.1% DMEM Advanced®[23], 37.1% DMEM medium[24], 10% antibiotics/antimycotics solution (0.1 g of penicillin A[25], 1 ml of gentamicin[26] at 50 μg/ml and 0.3 ml of anfotericin B[27] at 1 mg/ml for 100 ml of PBS), 15% Qualified Fetal Bovine Serum®[28], 0.4% L-glutamine[29], and 0.4% non-essential amino acids solution[30]. Culture flasks were stored at 37° C and 5% CO_2 and culture media was refreshed every 2 or 3 days. Passages were made when observed approximately 80-90% cell confluence, always respecting the density of 4,000 cells/cm^2. Fourth passage cells were used to induce differentiation into osteogenic, chondrogenic and adipogenic lineages following the suggestions of Sarugaser et al. (2009).

[23] 12491015, Gibco, U.S.A.
[24] 12561056, Gibco, U.S.A.
[25] P3032, Sigma-Aldrich, U.S.A.
[26] G1397, Sigma-Aldrich, U.S.A.
[27] A9528, Sigma-Aldrich, U.S.A.
[28] 12664025, Gibco, U.S.A.
[29] 59202C, Sigma-Aldrich, U.S.A.
[30] M7145, Sigma-Aldrich, U.S.A.

Biomaterials surface topography

HAP/SF composites (Fig. 1A) were made from a mix of 20% silk fibroin (Fig. 1B) and 80% synthetic hydroxyapatite[31] (Fig. 1C). X-ray diffraction was performed to determine the crystallinity of the composite. Pure samples of HAP and SF fibers were also analyzed as control. Surface topography of the composite and pure SF were analyzed by scanning electron microscopy (SEM).

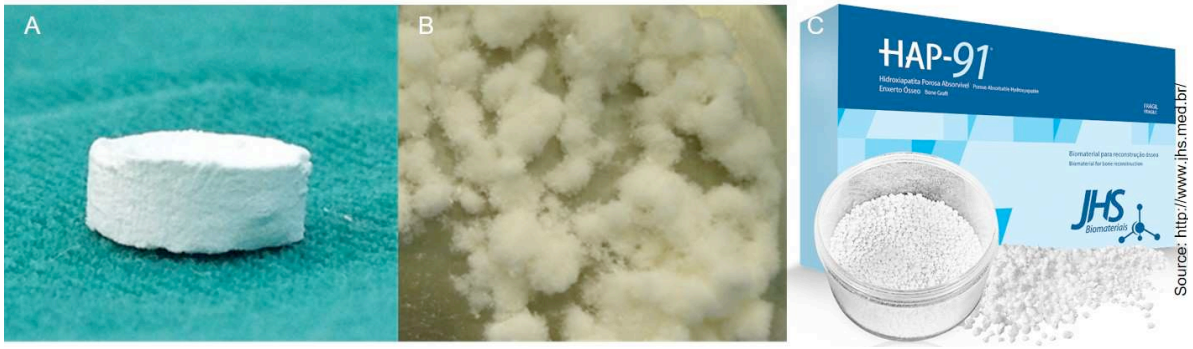

Figure 1. Macroscopic view of the HAP/SF composite (A), pure SF filaments (B) and pure HAP used in the in the biomaterials characterization.

Viability assay

To evaluate the effect of the HAP/SF composite on in vitro cell proliferation, a viability assay was performed culturing 2 x 10^4 human osteoblasts (HOBs) at sixth passage (p6) per well of 24 wells plates. Cells were cultured together with the composite for 1, 2 and 7 days (n=4) with DMEM media supplemented with 10% FCS and 1% antibiotics, with culture media refreshed every 2 or 3 days. Wells without the composite (n=4) were used as control. Once reached the time points, the cultured media was removed, the wells were carefully washed with PBS, plates were frozen at -80°C and then the CyQuant®[32] cell proliferation assay was performed following the manufacturer's recommendations. Briefly, HOBs at p6 and cultured in T75 flasks

[31]HAP-91®, JHS Chemistry Laboratory, Brazil.
[32]C7026, ThermoFischer Scientific, U.K.

were tripsinized and serial dilutions with known amounts of cells were prepared in duplicate. Next, a standard curve was prepared correlating the fluorescence emitted from those known amounts of cells and an equation was generated to transform the relative light units (rlu) emitted from the 96 wells plates into number of cells. Each 96 well plate was read 3 times by a luminescence plate reader[33]. Data were submitted to analysis of variance (two-way ANOVA), followed by pairwise comparisons test (Tukey test, $p<0.05$).

Reactive oxygen species (ROS) assay

For this assay, a commercial kit[34] was used to assess the real time leucocytes activation (ROS release) from peripheral blood of 4 different human donors. The donors were healthy and were not taking any prescription medications. The assay was carried out following manufacturer's instructions. Briefly, 20 µl of diluted blood (1:100) was placed in each well of a 96 well plate. Then, 20 µl of a solution containing 15 mg/mg of the composite was added to each well. In sequence, the adjuvant K® (signal enhancer) and the Pholasin® (chemiluminescent dye) were added. Using a luminescence plate reader with automatic injection[35], the 96 well plates were pre-incubated at 37° C for 30 minutes prior to addition of the tripeptide fMLP (formyl-methionyl-leucyl-phenylanine) in each well. Then, the emitted light generated due activation of leucocyte surface NADPH was measured every 10 seconds for 20 minutes; after that, the PMA (phorbol 12-merystate 13-acetate) reagent, a protein kinase C agonist, was injected and the luminescence generated by the extracellular leucocytes degranulation was recorded for more 30 minutes, providing a final total measure of the amount of ROS released during phagocytosis remaining in the cells after incubation with the biomaterial (BRYAN et al., 2012a). Each donor had their blood tested with the composite four times and the same number of wells per donor were used to test the leucocytes activation in the absence of the biomaterial

[33]FLUOstar OPTIMA, BMG Labtech, Germany.
[34]ABEL® Cell Activation Kits with Pholasin®, Knight Scientific, U.K.
[35]FDSS/µCell Functional Drug Screening System, Hamamatsu, Japan.

(reference controls). Incubations without blood and composite were also performed to confirm that the luminescence recording was directly related to the Pholasin® activation by secreted ROS. Once obtained the total ROS release pattern from the control references samples, it is possible to assess whether the biomaterial can enhance the generation of these free radicals which can be related to the failure of an implanted material (BRYAN et al., 2012a). Data were statistically analyzed by t student test ($p<0.05$).

Surgical procedure

For this experiment, it was used 27 New Zealand rabbits weighing on average 4 kg and 6 months aged. After premedication with tramadol hydrochloride (6 mg/kg/IM), general anesthesia induced with Tiletamine/zolazepam (30 mg/kg/IM) and maintained with isoflurane diluted in 100% oxygen, it was delimited a circular area in rabbits' skull using an 8 mm trephine drill coupled to an electric driller (Fig. 2A) at a speed of 5000 rpm and under continuous irrigation with sterile saline solution. The trephine was positioned at the center of the bregma region. Then, wear drills (Fig. 2B) connected to the same driller were used to abrade the bone tissue until meninges exposition throughout the extent of the defect be observed (Fig. 2C). Twenty-four animals were divided into 6 experimental groups according to the type of material implanted within the defects: allogenic MSCs only (G1); HAP/SF composite + MSCs (G2); pure SF filaments + MSCs (G3); unfilled defects (sham, G4); HAP/SF composite only (G5); pure SF filaments only (G6). Pure SF was used to evaluate whether it could have a bone healing potential by itself. For allogenic transplantation, a suspension with 1×10^6 cells in 0.3 ml of PBS was prepared for each animal, and the suspension was deposited directly onto meninges in G1 (Fig. 2D), and for G2 (Fig. 2E) and G3 (Fig. 2F), the defect was filled with their respective biomaterials and the suspension were deposited on top of them.

After filling the defects, the surgical wound was sutured with nylon 3-0 by a haemostatic suture standard. The animals were medicated with tramadol

hydrochloride (6 mg/kg/IM) every 12 hours for five days and enrofloxacine (5mg/kg/IM) every 24 hours for seven days.

MSCs tracking into bone defects

For G1, G2, and G3, it was included one more animal per group and these animals had the MSCs labelled with PKH26 membrane dye[36] before cell transplantation. Then, 15 hours after transplantation, the animals were euthanized with overdose of propofol and potassium chloride, the bone fragment containing the defect was removed using a cutting drill coupled to the electric driller and analyzed by confocal microscopy[37].

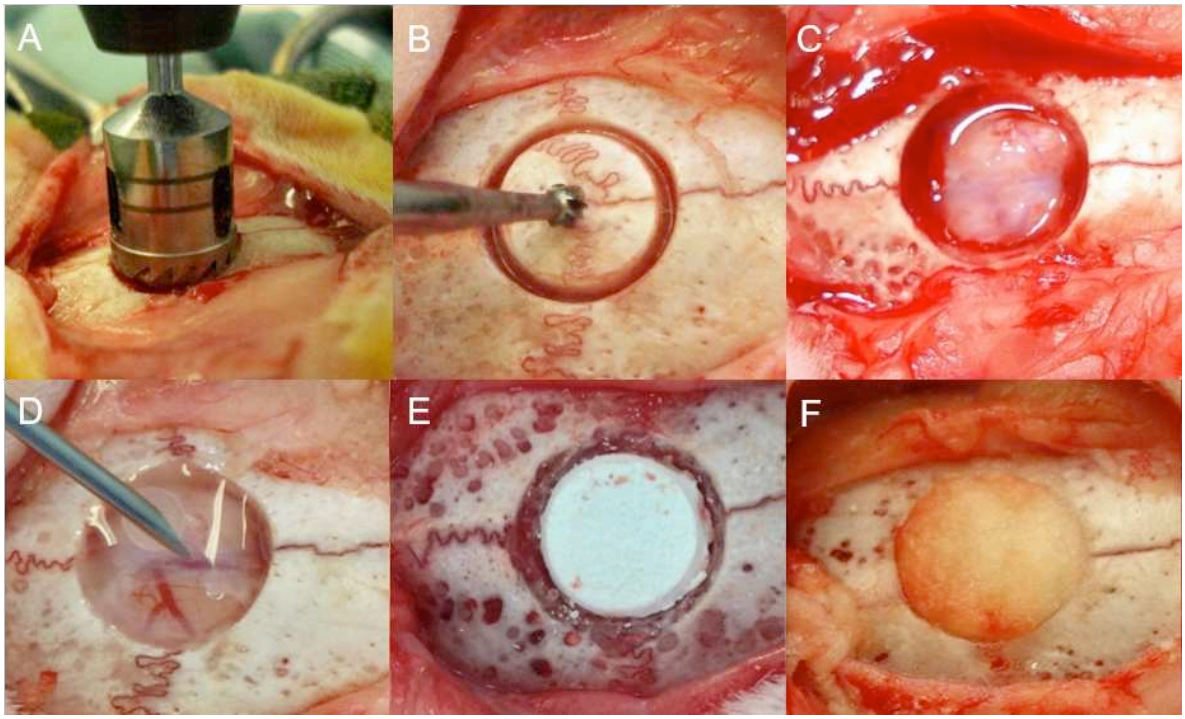

Figure 2. Surgical procedure illustrating the induction of an 8 mm diameter defect in the calvaria of rabbits and its treatment with MSCs and biomaterials. A – Delimitation of a circular area in the skull using an 8mm trephine drill coupled to an electric driller. B – Abrasion of the delimitated area using wear drills. C – Final aspect of the bone defect. D – Defect filling with the solution of MSCs in the absence of materials (G1). E – Defect filled with HAP/SF composite (G2) before receiving the cell suspension. F – Defect filled with SF filaments and MSCs (G3).

[36]MINI26-1KT, Sigma-Aldrich, U.S.A.
[37]LSM 510, Zeiss, Germany.

Clinical analysis

Post operatively daily assessment was performed for the first seven days, and then weekly until reaching 30 post-operative days. The wound appearance was assessed and the sensitivity reaction to digital touch of the calvaria was graduated in: 1 - no reaction; 2 - head retraction; and 3 - head retraction and movement. The wound appearance was evaluated by qualitative analysis and the sensitivity reaction was submitted to Tukey test post Kruskal-Wallis ($p < 0.05$).

Micro-computed tomography (µCT)

At the end of the trial period (30 days), animals were euthanized and a sample containing the defect was removed from each animal, both procedures were done in the same manner described previously for the MSCs tracking. The samples were fixed in 10% formalin, and after calibration of the micro-tomograph[38], the defects were scanned into 0.05 mm thick slices and qualitatively evaluated. Once all the samples were scanned, one sample of each group were addressed to X-ray diffraction and four to histological analysis.

X-ray diffraction (XRD) of the samples containing the defect

The region of the defect was removed and macerated, and then the XRD[39] was performed to analyze the crystallinity pattern inside the defects.

[38]Skyscan 1174, Bruker Corporation, U.S.A.
[39]X'Pert[3] Powder, PANalytical, Netherlands.

Histological analysis

Samples containing the defect were decalcified by solution of formic acid and sodium citrate, dehydrated, and embedded in paraffin. Histological cross sections were made with 8 μm of thickness. The sections were stained with hematoxylin and eosin and evaluated by light microscopy regarding to the bone healing. By histomorphometry with light microscope[40], camera[41], and specific software[42], the ratios of bone and provisory matrix formation in the defect area were estimated[43] and the results were evaluated by Tukey test post ANOVA ($p<0.05$).

RESULTS AND DISCUSSION

Biomaterials surface topography

As SF is a large molecule composed of 4.700 amino acid residues distributed between a crystalline and an amorphous portion (WEI et al., 2011), XRD of pure SF showed the presence of only one broad base peak approximately at the 2θ angulation of 20.5º (Fig. 3A), which is attributed to the structure of β-sheets that forms the crystalline portion of fibroin (KIM et al., 2005b) and was not detected in HAP/SF composite XRD (Fig. 3B). The same analysis demonstrated the presence of HAP characteristic peaks (Fig. 3C) in the HAP/SF composite (Fig. 3B), suggesting that composite maintained its crystallinity in a pattern similar to that observed for pure HAP. The attenuation or magnification of some HAP and SF characteristic peaks in the composite can be related to the biomaterial composition (80% HAP and 20% FS),

[40]Eclipse E600, Nikon, U.S.A.
[41]Digi-Pro 5.0M, Feldmann Wild Leitz, Brazil.
[42]Micrometrics® SE Premium, ACCU-SCOPE, U.S.A.
[43]Image Pro-Plus®, Media Cybernetics, U.S.A.

once the mix of materials with different characteristics can give a new crystallinity pattern to the resulting biomaterial (REY et al., 2005).

Scanning electron microscopy by secondary electrons revealed that both SF filaments (Figs. 4A and 4B) and HAP/SF composite (Figs. 4C and 4D) had surfaces that may be interesting for cell adhesion. SF filaments had an average diameter of 16 μM, and its conformation provided a network arrangement (Figs. 4A and 4B) similar to the arrangement described by Kim et al. (2005a), which could act as a support for cell containment, differentiation and proliferation (MIN et al., 2004). In the HAP/FS composite, a compact structure without spaces or pores suitable to cellular infiltration was observed (Fig. 4C); however, the presence of HAP at the surface could support the MSCs anchorage (WEBSTER et al., 1999) and contribute to their differentiation and proliferation (MURUGAN & RAMAKRISHNA, 2005).

Viability assay

Using the equation ($y = 0.7159x + 3494.3$) provided by the standard curve (Fig. 5) and the fluorescence light emitted (y) from the wells, the numbers of cells (x) in each well were obtained (Tab. 1). The Fig. 6 shows a higher number of cells (means) cultured in the presence of the composite than the reference control only after 1 culture day ($p<0.01$), and at the other time points the numbers of cells were very similar between the treatments. These results suggest that the composite does not have a deleterious effect on HOBs proliferation in vitro, and it could even have favored cell proliferation during the first 24 hours of cultivation. In addition, it is suggested that the composite might have provided a more stable cell proliferation from the second culture day onwards, once the standard deviations of cell numbers at 2 and 7 culture days (Tab. 1 and Fig. 6) were lowest when the cells were cultured with the biomaterial. The viability results for the composite agree with the studies developed by Liu et al. (2008), Andiappan et al. (2013), Gholipourmalekabadi et al. (2015), Jin et al. (2015). Lin et al. (2015), Yashi et al. (2015) and Shao et al. (2016),

who all investigated the effect of different compounding of HAP/SF materials on cell viability and found no deleterious effect.

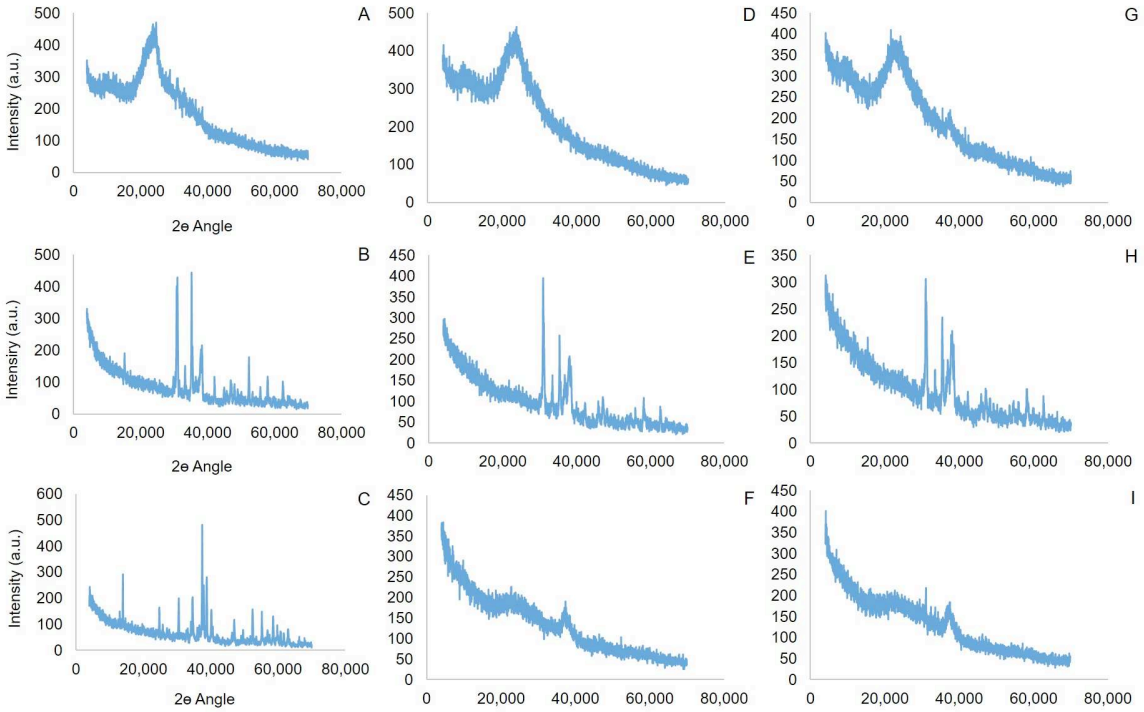

Figure 3. X-ray diffraction patterns of the biomaterials (HAP/SF composite, pure SF and pure HAP) and of the content filling the bone defects in G1, G2, G3, G4, G5 and G6 at 30 post-operative days. A - X-ray diffraction of SF filaments, showing only one broad basis peak, approximately at angle 20.5º, which cannot be detected in the HAP/ FS composite (B). B - X-ray diffraction of HAP/SF composite, showing crystallinity pattern similar to pure HAP (C). C - X-ray diffraction of pure HAP used as control. D - X-ray diffraction of a sample from G3 showing similar crystallinity pattern to pure SF. E - X-ray diffraction of a sample from G2 showing similar crystallinity pattern to HAP/SF composite. F - X-ray diffraction of a sample from G1 showing characteristic peaks of organic substances. G - X-ray diffraction of a sample from G6 showing crystallinity pattern similar to those observed for SF filaments (A) and for G3 (D). H - X-ray diffraction of a sample from G5 showing crystallinity pattern similar to those observed for the HAP/SF composite (B) and for G2. I - X-ray diffraction of a sample from G4 showing characteristic peaks of organic substances similar to those peaks observed for G1.

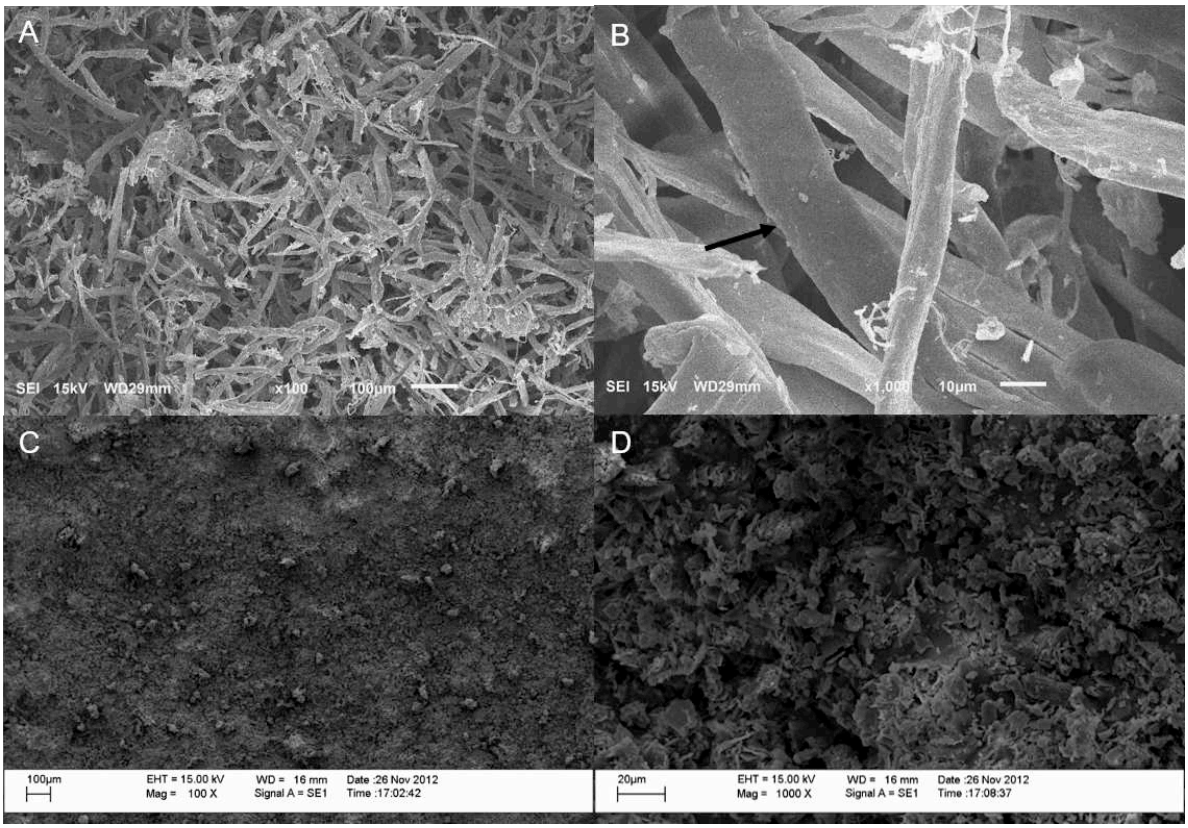

Figure 4. Images by scanning electron microscopy of pure SF filaments and HAP/SF composite materials. A - Network organization of SF filaments. B - Magnification of 4A, showing SF filaments with on average 16 µM diameter (arrow). C – HAP/SF composite presenting a compact aspect. D - Magnification of 4C illustrating the complex surface of the composite formed due the presence of HAP crystals.

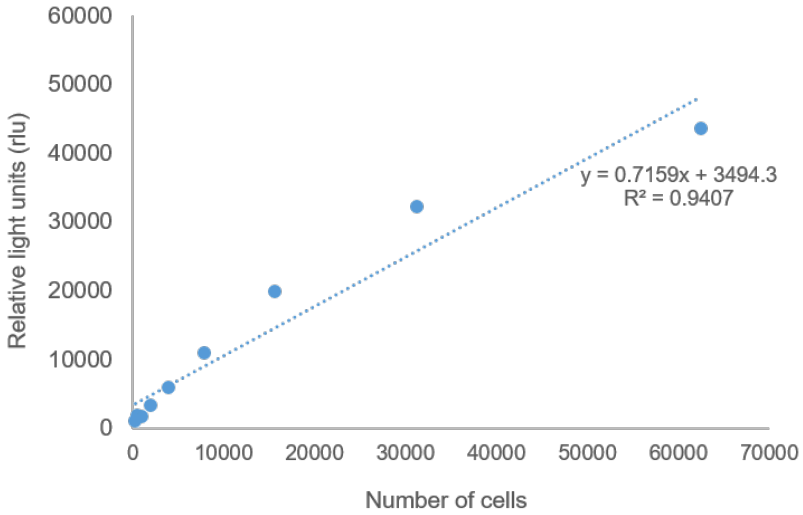

Figure 5. Graph ilustrating the HOBs stantard curve, which correlates the ligth emitted from the wells in relative ligth units (y) to number of cells (x) through the equation given (y=0.7159x + 3494.3) by a trendline.

Table 1. Luminescence data from three different plate readings of HOBs cultured on wells in the presence (n=4) and absense (n=4) of the HAP/SF composite, for 1, 2 and 7 days, converted to number of cells

	Culture days					
	Only HOBs (controls)			HOBs + HAP/FS		
	1	2	7	1	2	7
Reading 1 (well 1)	37880.57	58055.18	72865.90	57001.96	61679.98	60418.63
Reading 1 (well 2)	44938.82	58122.22	58313.59	59102.81	62381.20	69840.34
Reading 1 (well 3)	43088.00	49277.41	74857.80	63178.80	65490.57	72808.63
Reading 1 (well 4)	48092.89	69465.99	78549.66	60021.93	50442.38	67186.34
Reading 2 (well 1)	36363.60	57007.54	71044.42	54230.62	59633.61	59468.78
Reading 2 (well 2)	43801.79	56775.67	56824.56	57548.12	61667.41	69330.49
Reading 2 (well 3)	41864.37	47729.71	73930.30	61716.30	62100.43	72439.87
Reading 2 (well 4)	46687.67	68389.02	77868.00	57848.44	49012.01	64947.20
Reading 3 (well 1)	35436.09	54704.15	69239.70	52550.22	57631.93	57162.59
Reading 3 (well 2)	42512.50	56387.34	55968.29	56601.06	59377.99	67455.93
Reading 3 (well 3)	40713.37	47007.54	72544.63	59657.35	60552.73	71117.06
Reading 3 (well 4)	46193.18	67245.01	75234.95	56601.06	47711.55	63652.33
Mean	42297.74	57513.90	69770.15	58004.89	58140.15	66319.02
Standard deviation	-981.80	2424.24	2887.69	-2027.23	700.58	124.74

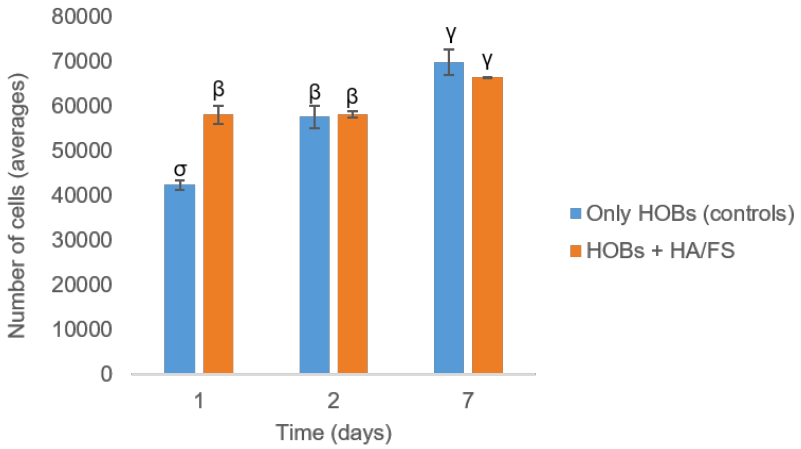

Figure 6. Number of HOBs (means) on wells cultured in the presence (n=4) and absense (n=4) of the HAP/SF composite for 1, 2 and 7 days. Symbols (σ, β and γ) represent groups statistically homogeneous. Error bars represent standard deviation from the mean.

ROS assay

The ROS investigation is a useful tool to predict in vitro a host response to biomaterials (BRYAN et al. 2012b) and this assay was performed here to evaluate whether an immune response could be triggered by the HAP/SF composite when in contact to human blood.

An example of the ROS kinetics recording is shown in Fig. 7, which demonstrates the generation of reactive oxygen species by leucocytes in response to material stimulation.

Fig. 8 illustrates the mean luminescence recorded from leukocytes activation of blood from the four donors incubated in the presence or absence of HAP/SF composite; the figure demonstrates that there was no statistically difference ($p=0.076$) between the amount of ROS released by untreated and HAP/SP-treated samples, suggesting that the composite did not increase the leukocyte ROS production.

Although it was not found in the literature references about leukocyte ROS response to a similar HAP/SF composite, results of the present study can be supported by studies with the two substances separately, like that developed by Albrech et al. (2009), who did not detect increase of ROS production by primary macrophages treated with hydroxyapatites of different physicochemical properties. However, Mestres et al. (2015) highlighted that is still possible to have macrophage activation by some hydroxyapatites on different levels and it could be mainly attributed to topographic differences rather than ionic exchanges with the surrounding media.

In turn, Park et al. (2011) suggested that the silk fibroin did not increase ROS production by pancreatic β-cells; although they used a different cell type for the assay, the comparison between the studies might be still valuable, once both pancreatic β-cells and phagocytes can release ROS by the same NADPH oxidase system (OLIVEIRA et al., 2003). Besides, using a different approach based on nitric oxide production and TNF-α release to assess macrophage activation, Acharya et al. (2008) also suggested that the silk fibroin proteins can be immunologically inert and might invoke minimal immune response.

Data in Fig. 9 shows the mean of ROS production in response to the HAP/SF composite for each donor, demonstrating significant differences between donors according to the level of leukocytes activation. Donors 1 and 2 had similar responses, while donors 3 and 4 were shown to have had greatest leukocytes activation. According to Bryan et al. (2012b), different levels of leucocytes activation between donors are expected and they reflect the potential for variations in trans-donor response to an implanted biomaterial.

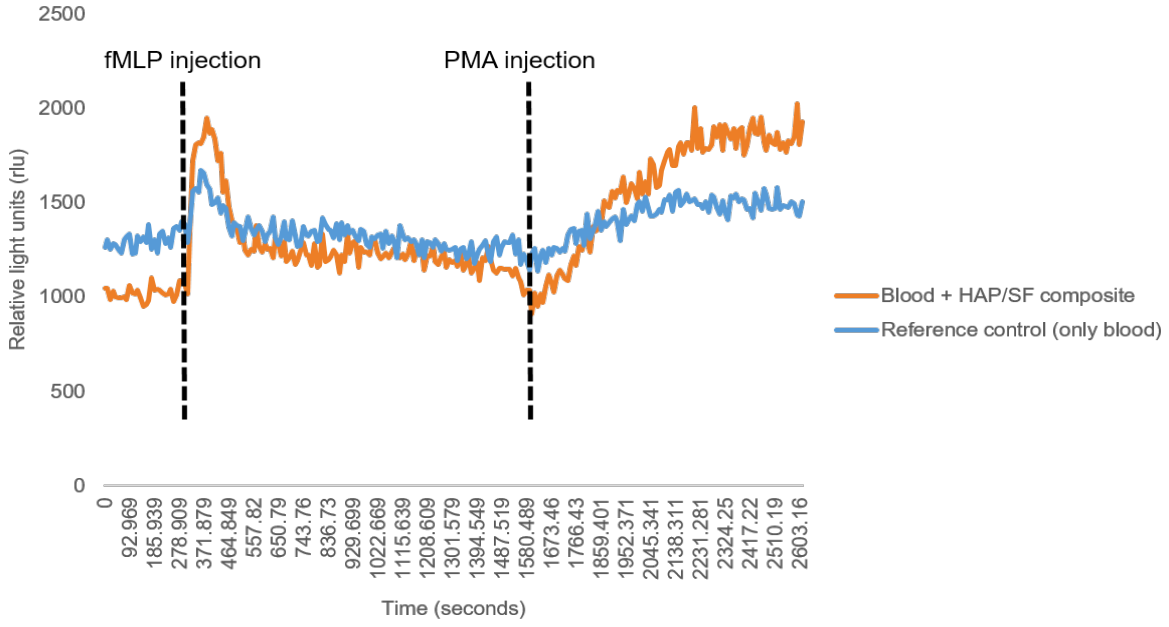

Figure 7. Example of the chemiluminescent recording of leucocyte ROS production during the incubation of diluted blood with HAP/SF composite. Lines represent a mean value (n=4) and the recordings were performed every 10 seconds.

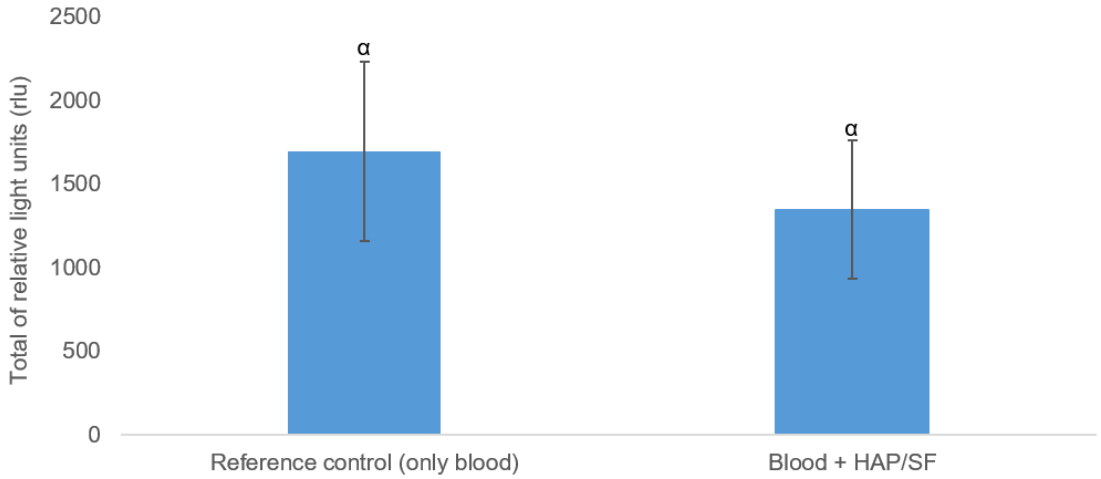

Figure 8. Mean of ROS released from leukocytes of whole blood incubated in the presence and in the absence of HAP/SF composite. Symbols (α) represent groups statistically homogeneous. Error bars represent standard deviation from the mean, n=16 (4 donors x 4 experimental repeats).

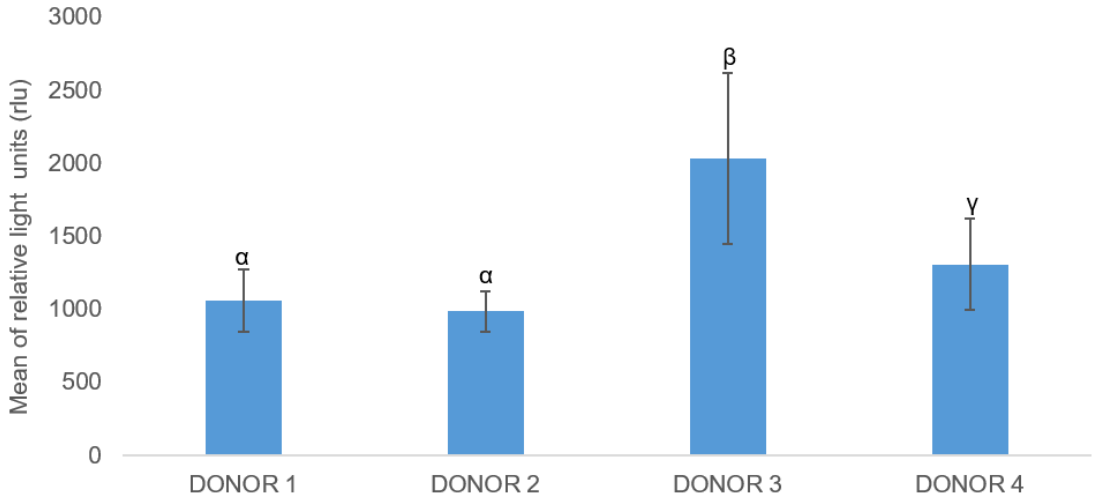

Figure 9. Mean of ROS production in response to the HAP/SF composite for each donor. Symbols (α, β and γ) represent groups statistically homogeneous. Error bars represent standard deviation from the mean, n=4.

MSCs tracking into bone defects

Tissue analysis 15 hour post-implantation showed the sustained presence of MSCs in all defects (Fig. 10); however, the number of MSCs per field of view was higher in the defect filled with HAP/SF composite before receiving cell transplantation. This analysis reflects the importance of including a scaffold into cell

therapy techniques in order to maintain the cells at a determined reparation-target site (BAČÁKOVÁ et al., 2004; PRESTWICH & HEA, 2015); HAP/SF composite was shown to do it better than pure SF filaments within the first 15 hours post cell transplantation, probably due the complexity provided by HAP to the composite surface.

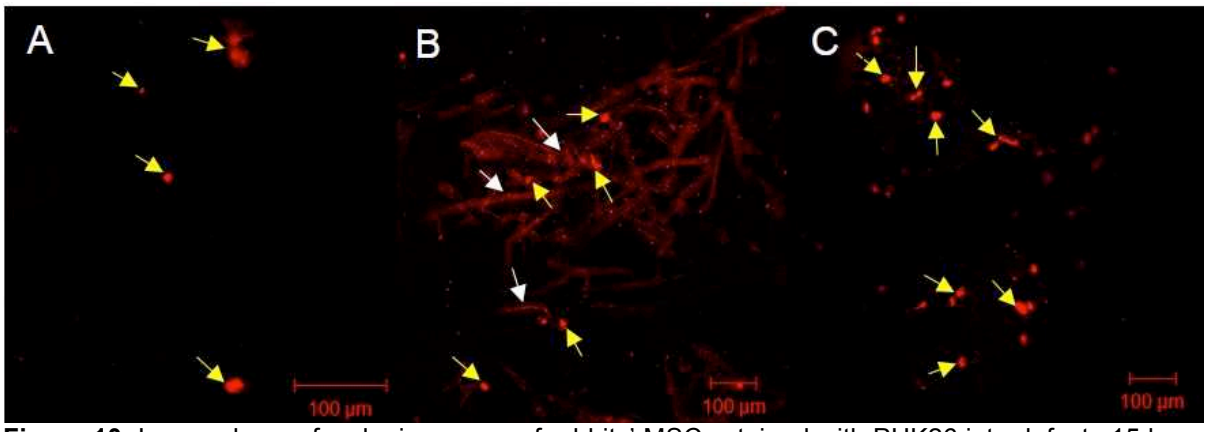

Figure 10. Images by confocal microscopy of rabbits' MSCs stained with PHK26 into defects 15 hours after the transplantation. A – Isolated cells (yellow arrows) into defect of group 1 (only MSCs). B – MSCs (yellow arrows) in contact with SF filaments (white arrows), which have natural fluorescence. C – MSCs aggregates (yellow arrows) on top of the HAP/SF composite.

Clinical analysis

None of the rabbits showed infection, dehiscence, neurological abnormalities nor purulent inflammatory reaction around surgical site, as well as reported by Hofmann et al. (2013), who worked with a SF scaffold in mice, and by Park et al. (2015) assessing a HAP/SF biomaterial in rabbits, both of them using the same model of bone defect reported in the present study. Fig. 11 evidences that all animals presented, on average, sensitivity pain at third degree of the scale on the first post-operative day. In G1 (only MSCs) and G4 (sham), animals had their pain graduation decreased in a full degree after four post-operative day onwards; animals from G2 (MSCs + HAP/SF) had the same reduction only after 7, while those from G3 (MSCs + SF) after 6, and those from G5 (HAP/SF) and G6 (SF) after 5 post-operative day onwards. There was no statistic difference between the treatment groups, which

means that the treatment with the biomaterials combined or not to MSCs did not influence on the physiologic process of surgical trauma.

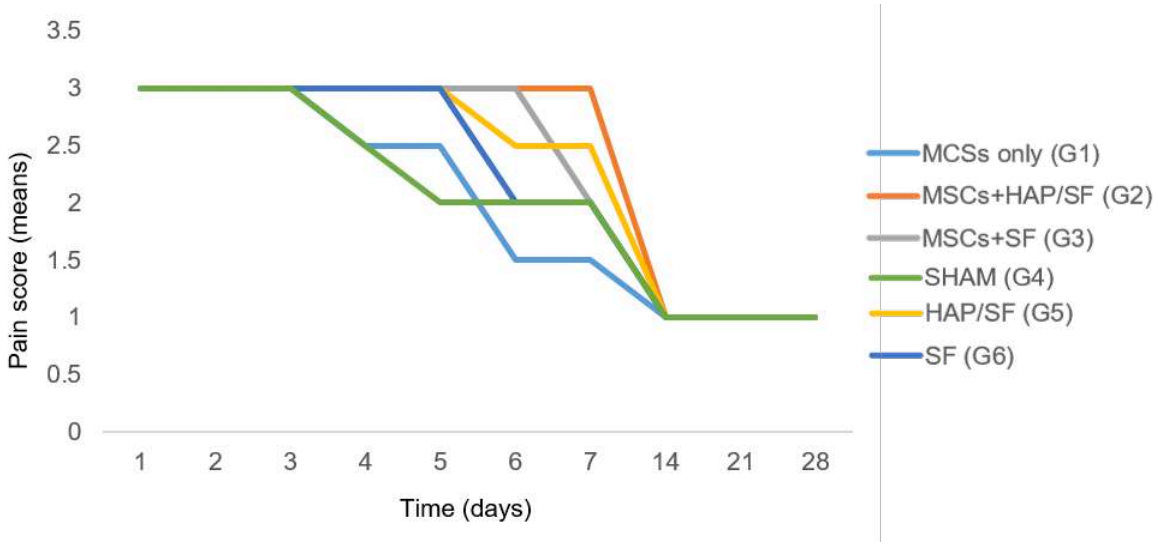

Figure 11. Graph illustrating the correlation between the pain score obtained from G1, G2, G3, G4, G5 and G6 along 30 post-operative days. Lines represent a mean value, n=6/group.

µCT

The µCT images suggested that bone formation was better in G2 (MSCs + HAP/SF) than in the other groups, with a more visible area of new bone formation opposed to the HAP/SF composite, which can be noticed in the Figs. 12A to 12F. These findings were more visible when the radiopacity of the images was down regulated through the µCT software (Figs. 12G to 12L), suggesting that the tissue formed inside the defects had lower opacity than host bone and at the same time higher opacity than soft tissue. Longitudinal sections of the defects (Figs. 13A to 13F) confirmed superior repair pattern with trabeculae formation in G2. Moreover, the implant interface appeared to have more bone formation from the edges of the defects treated with MSCs (G1, G2 and G3) in comparison to their respective controls (G4, G5 and G6), which did not receive cell transplantation.

Zhao et al. (2009) and Wang et al. (2010) evaluated the effect of HAP/SF scaffolds on segmental bone defects reparation, in dogs and rabbits respectively;

they also observed more focus of bone formation at 30 post-implantation days by radiographic analysis when the material was combined to bone marrow mesenchymal stem cells. Although they used a different defect model, it was clearly shown the benefit in associating the undifferentiated cells to the biomaterial for bone repair.

In turn, Kweon et al. (2011), using a HAP/SF composite with similar properties and not associated to any type of cells to assess the repair of an identical 8 mm bone defect in calvaria of rabbits, did not observed the same multiple focus of bone formation by μCT analysis of treated and control animals at the same time point, even using youngest animals. Taken these results together, it is suggested that MSCs may have had a key role in the μCT aspect observed in the present study mainly for animals from G1 (only MSCs) and G2 (MSCs + HAP/SF composite).

Interestingly, Figs. 12 and 13 also show that bone formation was greater in G1 (only MSCs) than in G3 (MSCs + SF filaments). Besides, the pattern observed in G4 (sham) is very similar to that observed in G6 (only SF filaments). These findings could demonstrate that the SF filaments might have not contributed to increase the bone formation even when combined to MSCs, differently of HAP/SF composite, which may have stimulated the development of some small opaque points even when used to fill the G5 defects in the absence of MSCs. This finding does not translate the results of Song et al. (2011), who noticed multi-focus of bone formation within 8 mm diameter defects in rabbits' skull treated with silk fibroin membranes by μCT analysis at the same time point. Albeit these authors used youngest animals in this study (3-month old animals), the main reason of the difference observed between the studies is probably based on the biomaterials production providing two silk fibroin materials with totally different surface topographies; as a result, the final biomaterial properties may be different and reflect distinct abilities in evoking bone healing.

XRD of the samples containing the defect

XRD showed characteristic peaks of the biomaterials used in the respective groups and organic peaks in G1 (only MSCs) and G4 (sham) (Figs. 3D to 3I), confirming that the biomaterials implanted were still within the defects at 30 post-operative days.

Histological analysis

As seem before by the μCT and XRD, the histological analysis also demonstrated that complete repair with bone did not occur in none of the defects. Thus, it was possible to analyse early tissue reparation process, where MSCs could have had a favourable role. In the groups that received only the MSCs (G1, Figs 14A to 14C) or no treatment (G4, Figs 14D to 14F), a provisional bone matrix and soft connective tissue formed from the bottom of the defect was observed. In the groups that received biomaterials (Figs 15 and 16), the defects were predominantly filled by the implanted material; soft tissue was present only on the top of the biomaterial in these groups as shown in Fig. 16A, ant it probably came from subcutaneous tissues. It was also observed that both the composite and the SF filaments used in this study could be biodegradable due to the presence of multinucleated giant cells interacting with the biomaterials (Figs. 15B and 16D). Also, they could interact with host bone with no fibrous soft tissue interposition (Figs. 15C and 16C). Fig. 17 clearly evidences the superior aspect of trabecular reorganization on the edges of defects, which received MSCs treatment, especially in G2 defects.

Tab. 2 illustrates the histomorphometric results and shows different percentages values (means) of bone formation and provisory matrix areas between the experimental groups. Although G2 (MSCs + HAP/SF) and G1 (only MSCs) had, respectively, the highest means of bone and provisory matrix formations (Fig. 18), statistical analyses demonstrated significant difference ($p<0.01$) only between G2

when compared to G4 (sham) and G6 (SF) for bone formation (Fig. 18A); for provisory matrix formation (fig. 18B), there were significant differences ($p<0.01$) between G1 and all the other groups, except for G4.

Taking the histological and histomorphometric results together, it is suggested that when MSCs were transplanted without biomaterials, provisory matrix formation could be stimulated to form new bone, but this new bone formation could be accelerated and the rate improved when the HAP/SF composite was associated to MSCs.

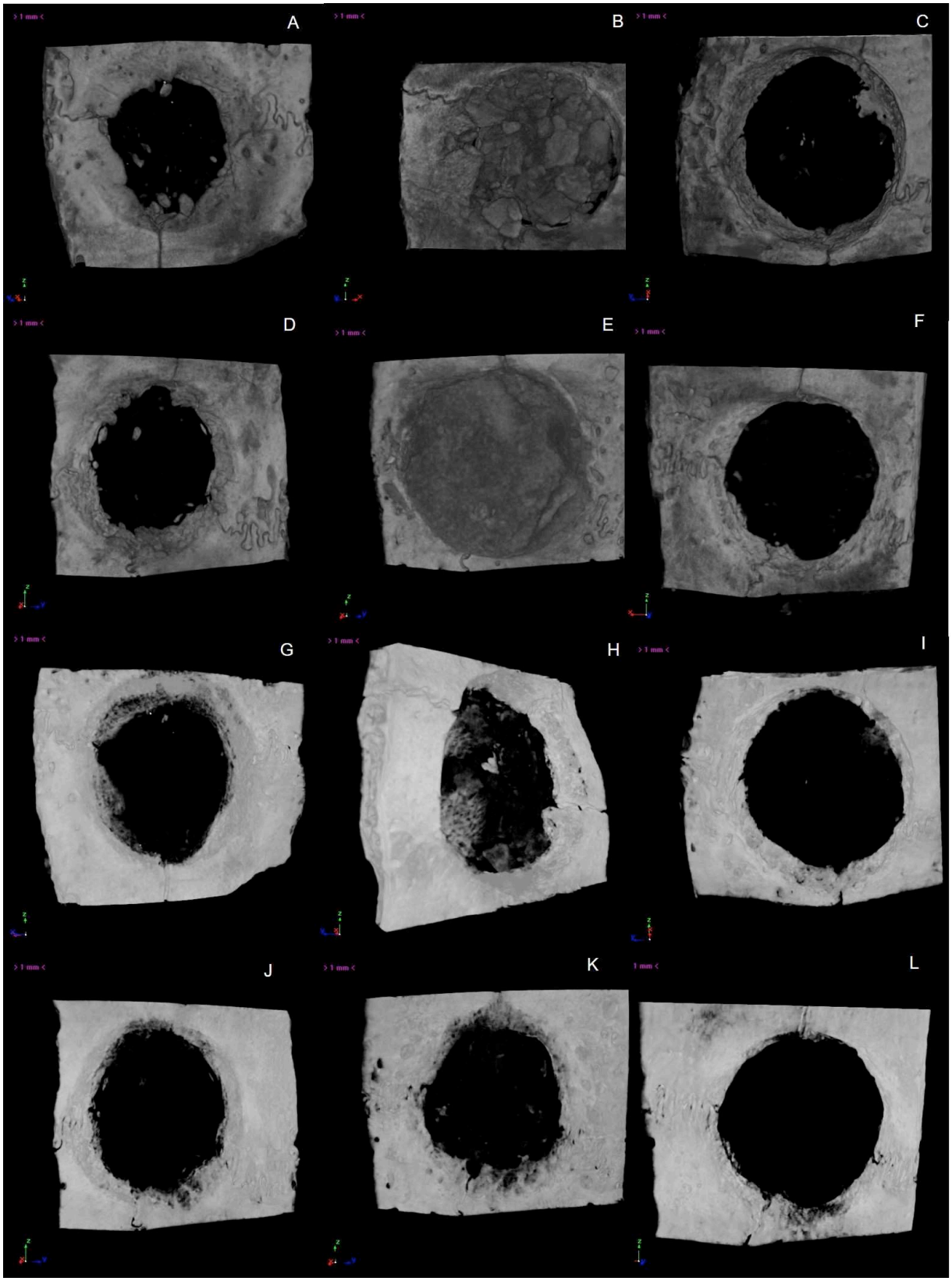

Figure 12. Images by µCT of the defects in rabbits' calvaria at 30 post-operative days. A – G1 (only MSCs). B – G2 (MSCs + HAP/SF). C – G3 (MSCs + SF). D – G4 (sham). E – G5 (HAP/SF). F – G6 (SF). Note the bone formation on the edge of the defects was more visible when radiopacity was down regulated, being possible more areas of bone formation in G1 (G) and G2 (H) than in G3 (I), G4 (J), G5 (K) and G6 (L).

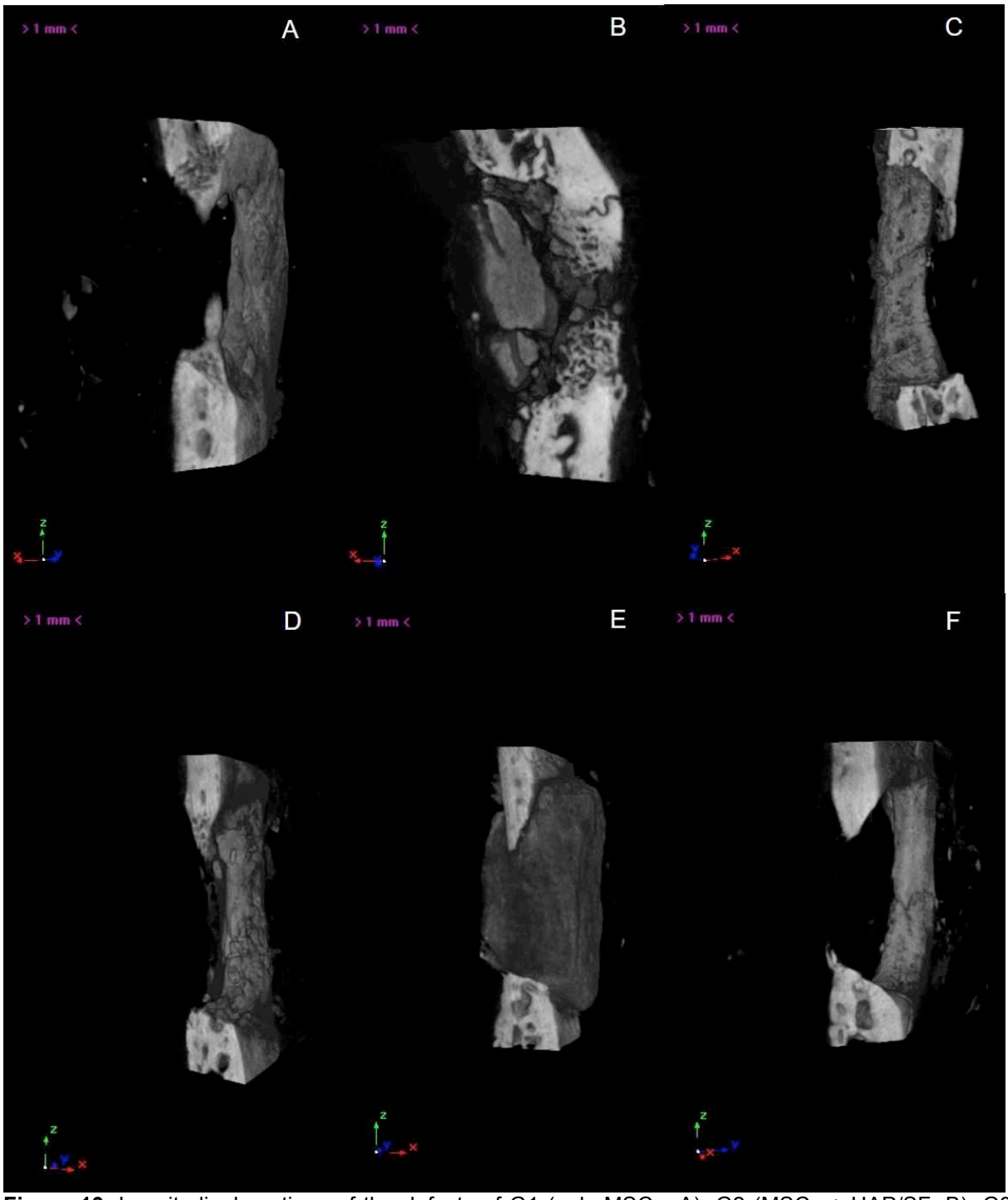

Figure 13. Longitudinal sections of the defects of G1 (only MSCs, A), G2 (MSCs + HAP/SF, B), G3 (MSCs + SF, C), G4 (sham, D), G5 (HAP/SF, E) and G6 (SF, F) at 30 post-operative days by µCT. Note the greatest bone formation on the edges of the defects in G1, G2 and G3 and the superior repair pattern with new trabeculae formation on the edges of a defect from G2.

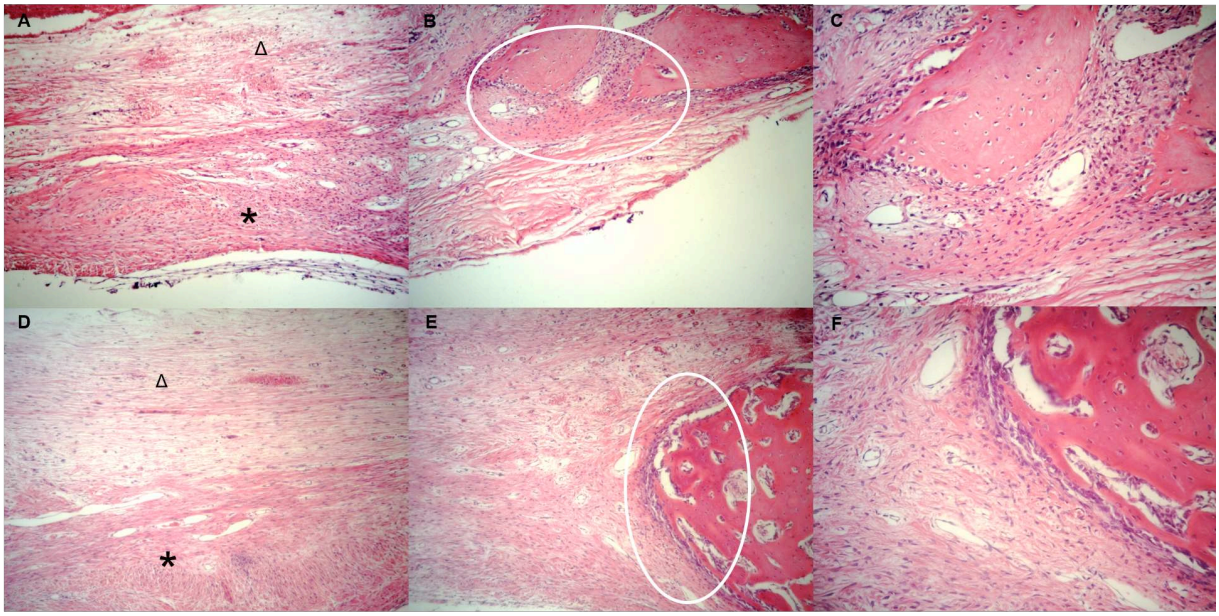

Figure 14. Photomicrographs illustrating histological findings of G1 (only MSCs) and G4 (sham) defects at 30 post-operative days. A - Presence of connective tissue (Δ) and provisional matrix (*) within a G1 defect. 100X. B - Bone formation (circled area) on the edges of a G1 defect. 100X. C - Magnification of the demarcated area in B. 200X. D – Presence of provisional matrix (*) and an apparent biggest area of connective tissue (Δ) within a G4 defect. E - Bone formation (circled area) within a G4 defect. 100X. F - Magnification of delimited area in E. 200X.

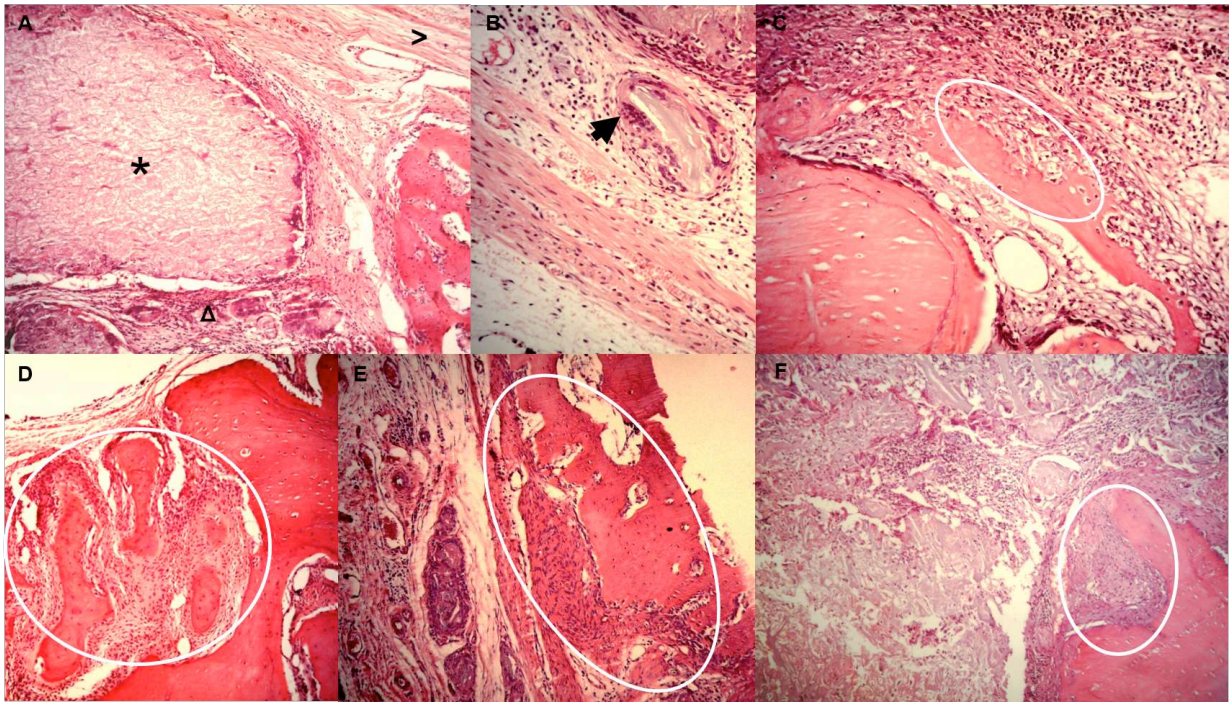

Figure 15. Photomicrographs illustrating histological findings of G2 (MSCs + HAP/SF) and G5 (HAP/SF) defects at 30 post-operative days. A - Defect predominantly filled by HAP/SF composite (*) in a G2 animal. Note presence of connective tissue deposition (>), probably from subcutaneous tissue, only on the composite surface, and areas with biomaterial degradation aspect (Δ) by phagocytic cells, mainly in the bone-biomaterial interface. 100X. B - Magnification of A, indicating composite degradation by giant cells (arrow). 200X. C – Interface showing HAP/SF composite interaction with the host bone (circled area) without fibrous tissue interposition. 200X. D - Area of intense trabecular reorganization on the edges of a G2 defect. 100X. E and F: histological aspects of G5 defects, indicating an inferior trabecular reorganization pattern (circled areas) in comparison to the same region in G2 defects. 100X.

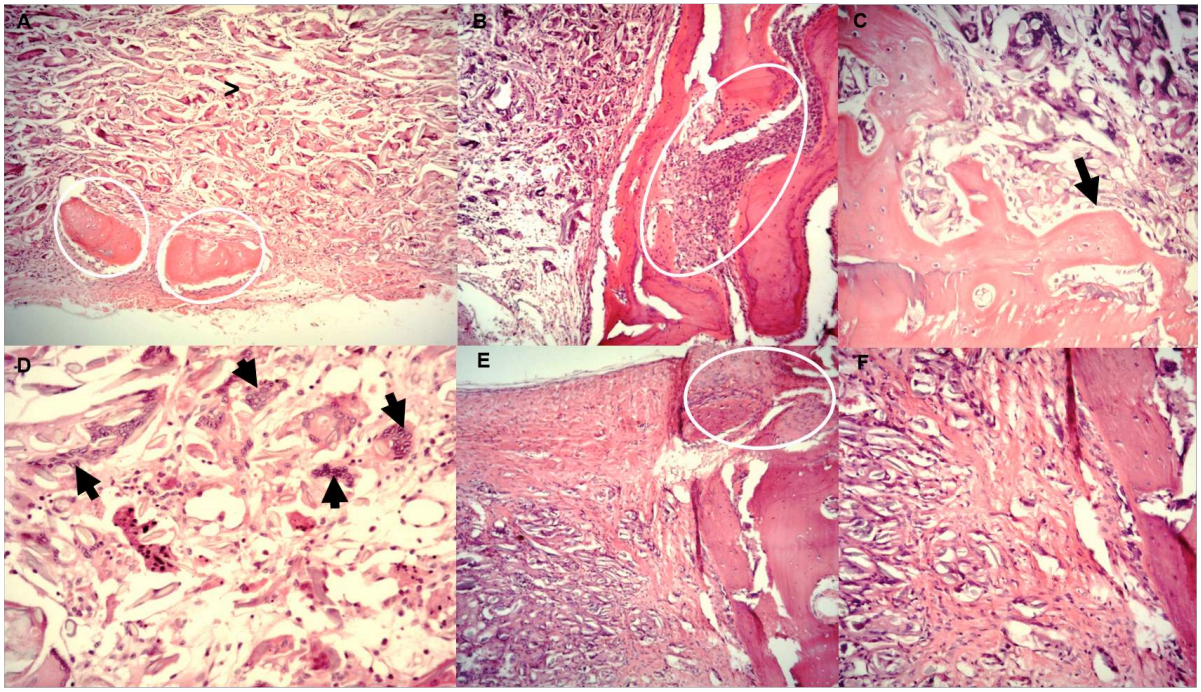

Figure 16. Photomicrographs illustrating histological findings of G3 (MSCs + SF) and G6 (SF) defects at 30 post-operative days. A - Presence of islands of bone formation (circled areas) circulated between the SF filaments within a G3 defect. 100X. B - Trabecular reorganization on edge of a G3 defect (circled area). 100X. C - Interface showing interaction between SF filaments and host bone (arrow) without fibrous tissue interposition. 200X. D – Presence of multinucleated giant cells (arrows) interacting with the SF filaments. 200X. E - Bone formation area (circled area) on the edge of a G6 defect. 100X. F - Magnification of E, showing the predominance of a temporary matrix (circled area) next to the trabecular region. 200X.

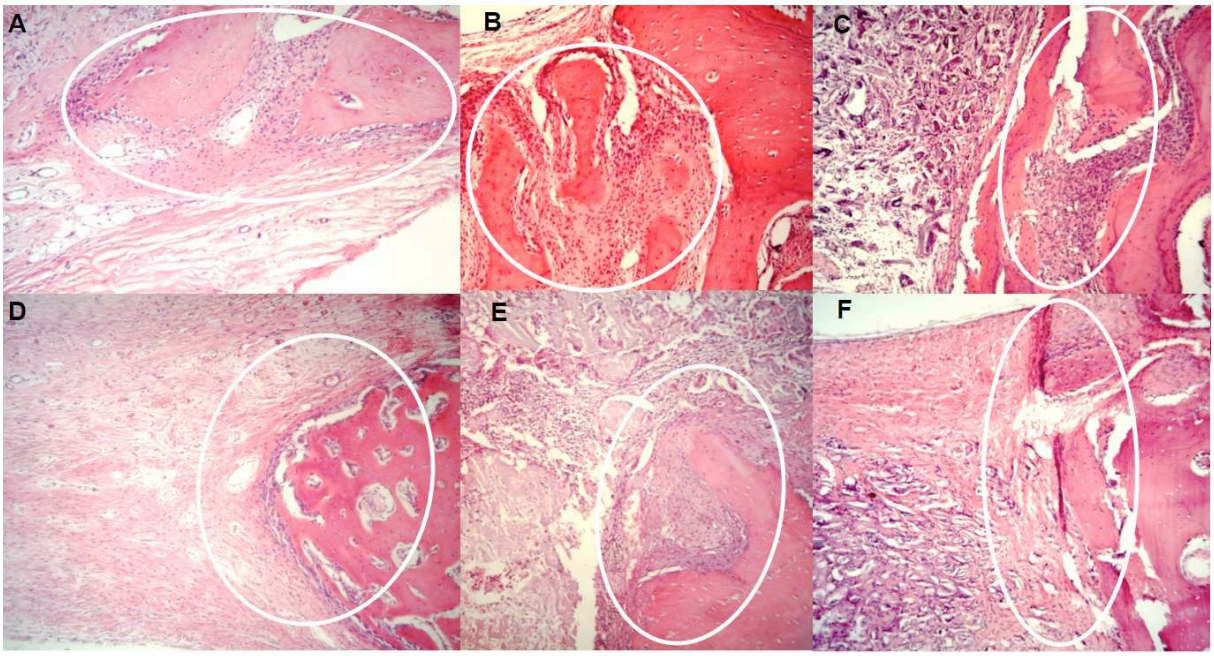

Figure 17. Photomicrographs illustrating the trabecular reorganization (circled areas) within G1 (only MSCs, A), G2 (MSCs + HAP/SF, B), G3 (MSCs + SF, C), G4 (sham, D), G5 (HAP/SF, E) and G6 (SF, F) defects at 30 post-operative days. Note more evident trabecular reorganization in B.

Table 2. Histomorphometric data (means) extracted from the region of the defects in G1 (only MSCs), G2 (MSCs + HAP/SF), G3 (MSCs + SF), G4 (sham), G5 (HAP/SF) and G6 (SF) at 30 post-operative days, n=4/group

	Experimental groups					
	G1	G2	G3	G4	G5	G6
Bone formation	12.34	21.57	12,6	5.72	12.21	7.23
Standard deviation	6.39	5.16	3.66	5.72	6.84	1.88
Provisory matrix	41.20	16.26	12.6	33.29	2.54	14.06
Standard deviation	12.73	5.06	3.66	4.78	4.27	9.41

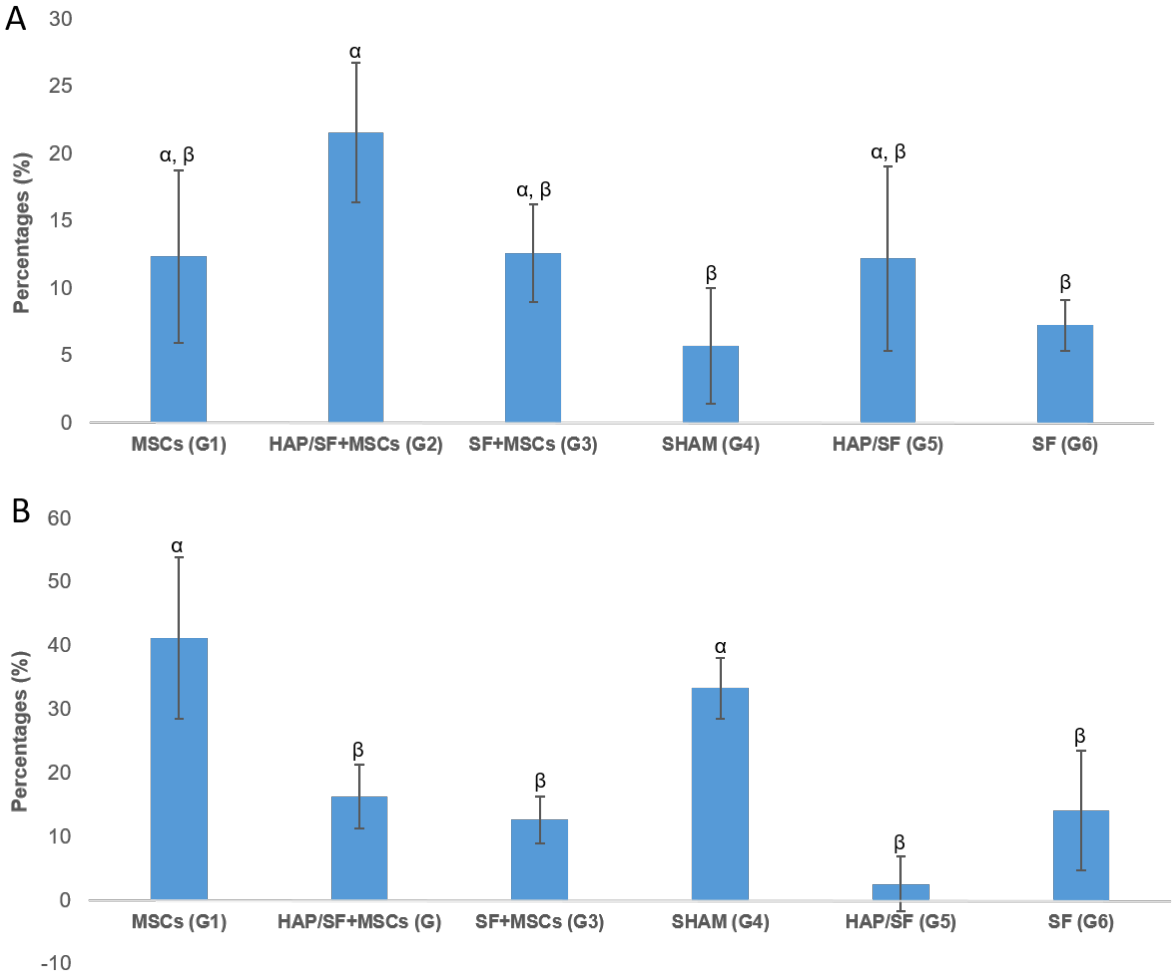

Figure 18. Mean values of bone (A) and provisory matrix (B) percentages within G1, G2, G3, G4, G5 and G6 defects at 30 post-operative days. Symbols (α and β) represent groups statistically homogeneous. Error bars represent standard deviation from the mean, n=4.

Similar studies using a mice model to evaluate the osteogenic potential of mesenchymal stem cells also noticed a superior pattern of bone formation at 30 (MONTEIRO et al., 2012) and 56 (SEO et al., 2008) days after cell transplantation into calvaria defects. According to Horie et al. (2012), the therapeutic effect of stem cells on bone healing may be mainly based on the paracrine signalling, once the survival and differentiation of implanted MSCs into bone defects would be limited. This supposition is strongly supported by studies of bone repair via paracrine signalling induced by stem cells conditioned media. In these studies, the cultured media in which the stem cells grow and release various cytokines is processed, then it is implanted into bone defects without stem cells, providing an increased bone

repair and proving the paracrine effect (OSUGI et al., 2012). In addition, conditioned media of stem cells activated with inflammatory cytokines is proven to promote in vitro osteoblast proliferation, migration, differentiation and mineralization, culminating in an enhanced osteogenesis; this fact highlights the role of inflammation and paracrine signaling when the bone regeneration is guided by stem cells therapy (LI et al., 2016).

Among the cytokines secreted by stem cells, there are insulin-like growth factor 1 (IGF-1), transforming growth factor beta 1 (TGF-ß1), vascular endothelial growth factor (VEGF), bone morphogenetic protein 1 (BMP-1), interleukin 6 (IL-6), IL-3, monocyte chemoattractant protein 1 (MCP-1) and MCP-3. These immunomodulatory factors might have specific roles in the bone repair; IGF-1 can induce osteoblast proliferation and migration; TGF-ß1 can recruit osteoprogenitor cells and stimulate their proliferation and differentiation; VEGF is believed to be the main regulator of angiogenesis, contributing to osteogenesis, and BMP-1 has an important role in the development of cartilage and bone. In turn, MCP-1 and 3 and interleukins 3 and 6 are shown to be important in the recruitment of endogenous stromal cells and endothelial cells respectively, and these interleukins can also induce osteogenic differentiation (LINERO & CHAPARRO, 2015). Equally important is the presence of resident mesenchymal stem cells within the cranial sutures, which also participates in this signalling for craniofacial bone turnover and injury healing (ZHAO et al., 2015).

On the other hand, the HAP/SF composite can have had a synergic effect on this complex osteogenic environment, once HAP can guide the deposition of newly formed bone mineral (BHUMIRATANA et al., 2011), bonding directly to host bone; whilst natural organic polymers, like SF, can facilitate the cell growth and enhance the mechanical properties of the composite, improving the osteoinductive potential, biocompatibility, bioabsorbability and vascularization (JIN et al., 2014).

CONCLUSION

The results of this study suggested that the HAP/SF composite developed is biocompatible and avoided deposition of fibrous tissue within defects in calvaria of rabbits. When the MSCs were transplanted alone, the provisory matrix formation could be stimulated to form new bone on the edges of the defect, but this new bone formation might have been accelerated and the rate improved when the HAP/SF composite was implanted combined to MSCs.

REFERENCES

ACHARYA, C.; GHOSH, S.K.; KUNDU, S.C. Silk fibroin protein from mulberry and non-mulberry silkworms: cytotoxicity, biocompatibility and kinetics of L929 murine fibroblast adhesion. **The Journal of Materials Science: Materials in Medicine,** v. 19, p. 2827–2836, 2008.

ALBRECH, C.; SCHERBART, A.M.; VAN BERLO, D. et al. Evaluation of cytotoxic effects and oxidative stress with hydroxyapatite dispersions of different physicochemical properties in rat NR8383 cells and primary macrophages. **Toxicology in Vitro,** v. 23, p. 520–530, 2009.

BAČÁKOVÁ, L.; FILOVÁ, E.; RYPÁČEK, F. et al. Cell adhesion on artificial materials for tissue engineering. **Physiological Research,** v. 53, p. S35-S45, 2004.

ANDIAPPAN, M.; SUNDARAMOORTHY, S.; PANDA, N. et al. Electrospun eri silk fibroin scaffold coated with hydroxyapatite for bone tissue engineering applications. **Progress in Biomaterials,** v. 2, p. 1-11, 2013.

BHUMIRATANA, S.; GRAYSON, W.L.; CASTANEDA, A. et al. Nucleation and growth of mineralized bone matrix on silk-hydroxyapatite composite scaffolds. **Biomaterials,** v. 32, p. 2812-2820, 2011.

BORGES, A.P.B.; REZENDE, C.M.F.; RIBEIRO, M.F.B. et al. Hidroxiapatita sintética como substituto ósseo em defeito experimental provocado no terço proximal da tíbia em cão: aspectos à microscopia eletrônica de transmissão. **Arquivo Brasileiro de Medicina Veterinária e Zootecnia,** v. 52, 2000. Available on: <http://www.scielo.br/scielo.php?script=sci_arttext&pid=S010209352000000600011> . Access on: 06 Nov. 2014.

BRYAN, N.; ASWIN, H.; SMART, N.; et al. Reactive oxygen species (ROS) – A family of fate deciding molecules pivotal in constructive inflammation and wound healing. **European Cells and Materials,** v. 24, p. 249-265, 2012a.

BRYAN, N.; ASWIN, H.; SMART, N.; et al. In vitro activation of human leucocytes in response to contact with synthetic hernia meshes. **Clinical Biochemystry,** v. 45, p. 672-676, 2012b.

CARLO, E. C.; MARTINEZ, M. M. M.; NEHME, R. C. et al. Compósito para fabricação de implantes reabsorvíveis para osteossíntese: avaliação da biocompatibilidade em coelhos. **Ciência Rural,** v. 39, p.135-140, 2009a.

CARLO, E. C.; BORGES, A. P. B.; DEL CARLO, R. J. et al. Comparison of in vivo properties of hydroxyapatite-polyhydroxybutyrate composites assessed for bone substitution. **Journal of Craniofacial Surgery,** v. 20, p. 853-859, 2009b.

CORRE, P.; MERCERON, C.; LONGIS, J. et al. Direct comparison of current cell-based and cell-free approaches towards the repair of craniofacial bone defects – A preclinical study. **Acta Biomaterialia,** v. 26, p. 306-317, 2015.

DAWSON, E.; MAPILI, G.; ERICKSON, K. et al. Biomaterials for stem cell differentiation. **Advanced Drug Delivery Reviews,** v. 60, p. 215–228, 2008.

DOROZHKIN, S.V.; EPPLE, M. Biological and medical significance of calcium phosphates. **Angewandte Chemie International Edition,** v. 41, p. 3130-3146, 2002.

FRANCO, K. L; BORGES, A. P. B.; VILÓRIA, M. I. V. et al. Hidroxiapatita sintética pura, hidroxiapatita sintética associada ao colágeno e hidroxiapatita sintética associada ao lipossoma como substitutos ósseos em defeitos provocados na tíbia de cães: aspectos da osteointegração à microscopia de luz transmitida. **Arquivo Brasileiro de Medicina Veterinária e Zootecnia,** v. 53, p. 1-7, 2001.

GHOLIPOURMALEKABADI, M.; MOZAFARI, M.; GHOLIPOURMALEKABADI, M. et al. In vitro and in vivo evaluations of three-dimensional hydroxyapatite/silk fibroin nanocomposite scaffolds. **Biotechnology and Applied Biochemistry,** v. 61, p. 441-450, 2015.

GRIFFITH, L.G.; NAUGHTON, G. Tissue engineering – current challenges and expanding opportunities. **Science,** v. 295, p. 1009–1014, 2002.

GU, Y.; CHEN, L.; YANG, H.L. et al. Evaluation of an injectable silk fibroin enhanced calcium phosphate cement loaded with human recombinant bone morphogenetic protein-2 in ovine lumbar interbody fusion. **Journal of Biomedical Research. Part A,** v.9 7a, p. 177-185, 2011.

HAIDAR, Z.S.; HAMDY, R.C.; TABRIZIAN, M. Delivery of recombinant bone morphogenetic proteins for bone regeneration and repair. Part B: Delivery systems for BMPs in orthopaedic and craniofacial tissue engineering. **Biotechnollogy Letters,** v. 31, p. 1825-1853, 2009.

HOFMANN, S.; HILBE, M.; FAJARDO, R.J. et al. Remodeling of tissue-engineered bone structures in vivo. **The European Journal of Pharmaceutics and Biopharmaceutics,** v. 85, p. 119-129, 2013.

HORIE, M.; CHOI, H.; LEE, R.H. et al. Intra-articular injection of human mesenchymal stem cells (MSCs) promote rat meniscal regeneration by being activated to express Indian hedgehog that enhances expression of type II collagen. **Osteoarthitis and Cartilage,** v. 20, p. 1197-1207, 2012.

JIN, Y.; KUNDU, B.; CAI, Y. et al. Bio-inspired mineralization of hydroxyapatite in 3D silk fibroin hydrogel for bone tissue engineering. **Colloids and Surfaces B: Biointerfaces,** v. 134, p. 339-345, 2015.

JIN, J.; WANG, J.; HUANG, J. Transplantation of human placenta-derived mesenchymal stem cells in a silk fibroin/hydroxyapatite scaffold improves bone repair in rabbits. **Journal of Bioscience and Bioengineering,** v. 118, p. 593-598, 2014.

KHAN, Y.; YASZEMSKI, M. J.; MIKOS, A. G. et al. Tissue engineering of bone: material and matrix considerations. **The Journal of Bone and Joint Surgery, American Volume***,* v. 90, p. 36-42, 2008.

KIM, K. H.; JEONG, L.; PARK, H. N. et al. Biological efficacy of silk fibroin nanofiber membranes for guided bone regeneration. **Journal of Biotechnology,** v. 120, p. 327-339, 2005a.

KIM, U. J.; PARK, J. Y.; KIM, H. J. et al. Three-dimensional aqueous-derived biomaterial scaffolds from silk fibroin. **Biomaterials,** v. 26, p. 2775–2785, 2005b.

KIM, S. S.; KANG, M. N.; LEE, K. Y. et al. Therapeutic effects of mesenchymal stem cells and hyaluronic acid injection on osteochondral defects in rabbits' knees. **Knee Surgery & Related Research,** v. 24, p. 164-172, 2012.

KOTOBUKI, N.; IOKU, K.; KAWAGOE, D. et al. Observation of osteogenic differentiation cascade of living mesenchymal stem cells on transparent hydroxyapatite ceramics. **Biomaterials,** v. 26, p. 779-785, 2005.

KWEON, H. Y.; LEE, K. H.; CHAE, C. H. et al. Development of nano-hydroxyapatite graft with silk fibroin scaffold as a new bone substitute. **Journal of Oral and Maxillofacial Surgery,** v. 69, p. 1578-1586, 2011.

LI, C.; LI, G.; ZHOU, T. et al. Paracrine effect of inflammatory cytokine-activated bone marrow mesenchymal stem cells and its role in osteoblast function. **Journal of Biosciences and Bioengineering,** v. 121, p. 213-219, 2016.

LIN, L.; HAO, R.; XIONG, W. Quantitative analyses of the effect of silkfibroin/nano-hydroxyapatite composites on osteogenic differentiation of MG-63 human osteosarcoma cells. **Journal of Bioscience and Bioengineering,** v. 119, p. 591-595, 2015.

LINERO, I.; CHAPARRO, O. Paracrine effect of mesenchymal stem cells derived from human adipose tissue in bone regeneration. **PloS ONE,** v. 9, 2015.

LIU, L.; LIU, J.; WANG, M. et al. Preparation and characterization of nano-hydroxyapatite/silk fibroin porous scaffolds. **Journal of Biomaterials Science Polymer Edition,** v. 19, p. 325-338, 2008.

MESTRES, G.; ESPANOL, M.; XIA, W. et al. Inflammatory Response to Nano- and Microstructured Hydroxyapatite. **PloS ONE,** v. 10, p. 1-20, 2015.

MIN, B. M.; LEE, G.; KIM, S. H. et al. Electrospinning of silk fibroin nanofibers and its effect on the adhesion and spreading of normal human keratinocytes and fibroblasts in vitro. **Biomaterials,** v. 25, p. 1289-1297, 2004.

MONTEIRO, B. S.; ARGÔLO-NETO, N. M.; NARDI, N. B. et al. Treatment of critical defects produced in calvaria of mice with mesenchymal stem cells. **Annals of the Brazilian Academy of Sciences,** v. 84, p. 841-851, 2012.

MURUGAN, R.; RAMAKRISHNA, S. Aqueous mediated synthesis of bioaresornable nanocrystalline hydroxyapatite. **Journal of Crystal Growth,** v. 274, p. 209-2013, 2005.

OLIVEIRA, H. R.; VERLENGIA, R.; CARVALHO, C. R. O. et al. Pancreatic β-cells express phagocyte-like NAD(P)H oxidase. **Diabetes,** v. 52, p. 1457-1463, 2003.

OSUGI, M.; KATAGIRI, W.; YOSHIMI, R. Conditioned media from mesenchymal stem cells enhanced bone regeneration in rat calvarial bone defects. **Tissue Engineering: Part A,** v. 18, p. 1479-1489, 2012.

PARK, H. J.; NAM, Y. Y., PARK, S-Y. et al. Silk fibroin has a protective effect against high glucose induced apoptosis in hit-t15 cells. **Journal of Biochemical and Molecular Toxicology,** v. 25, p. 238-243, 2011.

PARK, J-Y.; YANG, C.; JUNG, I-H. et al. Regeneration of rabbit calvarial defects using cells-implanted nano-hydroxyapatite coated silk scaffolds. **Biomaterials Research,** v.19, p. 2-10, 2015.

PRESTWICH, G. D.; HEALY, K. E. Why regenerative medicine needs an extracellular matrix. **Expert Opinion on Biological Therapy,** v. 15, p. 3-7, 2015.

REIS, E. C. C.; BORGES, A. P. B.; ARAÚJO, M. V. F. et al. Periodontal regeneration using a bilayered PLGA/calcium phosphate construct. **Biomaterials,** v. 32, p. 9244-9253, 2011.

REIS, E. C. C.; BORGES, A. P. B. ; CARLO, R. J. et al. Guided tissue regeneration using rigid absorbable membranes in the dog model of chronic furcation defect. **Acta Odontologica Scandinavica,** p. 1-9, 2013.

REIS, E. C. C.; BORGES, A. P. B; FONSECA, C. C. et al. Biocompatibility, osteointegration, osteoconduction, and biodegradation of a hydroxyapatite-polyhydroxybutyrate composite. **Brazilian Archives of Biology and Technology,** v. 53, p. 817-826, 2010.

REY, C.; COMBES, C.; DROUET, C. et al. Physico-chemical properties of nanocrystalline apatites: implications for biominerals and biomaterials. **Materials Science and Engeneering: C,** v. 27, p. 198-205, 2005.

SARUGASER, R.; ENNIS, J.; STANFORD, W. L. et al. Isolation, propagation, and characterization of human umbilical cord perivascular cells (HUCPVCs). **Stem Cells in Regenerative Medicine: Methods and Protocols,** v. 482, p. 269-279, 2009.

SEO, B. M.; SONOYAMA, W.; YAMAZA, T. et al. SHED repair critical-size calvarial defects in mice. Oral Diseases, v. 14, p. 428-434, 2008.

SHAO, W.; HE, J.; SANG, F. et al. Coaxial electrospun aligned tussah silk fibroin nanostructured fiber scaffolds embedded with hydroxyapatite–tussah silk fibroin nanoparticles for bone tissue engineering. **Materials Science and Engineering C,** v. 58, p. 342–351, 2016.

SONG, J-Y.; KIM, S-G,; LEE, J-W. Accelerated healing with the use of a silk fibroin membrane for the guided bone regeneration technique. **Oral Surgery, Oral Medicine, Oral Pathology, Oral Radiology, and Endodontology,** v. 112, p. e26-e33, 2011.

TANAKA, T.; HIROSE, M.; KOTOBUKI, N. et al. Nano-scaled hydroxyapatyte sheets support osteogenic differentiation of rat boné marrow mesenchymal cells. **Materials Science & Engineering C,** v. 27, p. 817-823, 2007.

VITAL, C. C.; BORGES, A. P. B. ; FONSECA, C. C. et al. Biocompatibilidade e comportamento de compósitos de hidroxiapatita em falha óssea na ulna de coelhos. **Arquivo Brasileiro de Medicina Veterinária e Zootecnia,** v. 58, p. 175-183, 2006.

WANG, G.; YANG, H.; LI, M. et al. The use of silk fibroin/hydroxyapatite composite co-cultured with rabbit bone marrow stromal cells in the healing of a segmental bone defect. **The Journal of Bone and Joint Surgery,** v. 92, p. 320-325, 2010.

WANG, M. Developing bioactive composite materials for tissue replacement. **Biomaterials,** v. 24, p. 2133-2151, 2003.

WEBSTER, T. J.; SIEGEL, R. W.; BIZIOS, R. Osteoblast adhesion on nanophase ceramics. **Biomaterials,** v. 20, p. 1221-1227, 1999.
WEI, K.; KIM, K. O.; NAKAGAWA, Y. et al. Fabrication of nano-hydroxiapatite on electrospun silk fibroin nanofiber and their effects in osteoblastic behavior. **Journal of Biomedical Material Research. Part A,** v. 97, p. 272-280, 2011.

YASHI, J.; KUNDU, B.; CAI, Y. et al. Bio-inspired mineralization of hydroxyapatite in 3D silk fibroin hydrogel for bone tissue engineering. Colloids and Surfaces B: **Biointerfaces,** v. 134, p. 339–345, 2015.

ZHAO, H.; FEGAN, J.; HO, T-V. The suture provides a niche for mesenchymal stem cells of craniofacial bones. **Nature Cell Biology,** v. 17, p. 386-396, 2015.

ZHAO, J.; ZHANG, Z,; WANG, S. et al. Apatite-coated silk fibroin scaffolds to healing mandibular Border Defects in Canines. **Bone,** v. 45, p. 517-527, 2009.

GENERAL CONCLUSION

The results of the study suggested that the techniques presented here provide a successful method for mesenchymal stromal cells isolation, expansion and characterization based on tri-lineage differentiation method. Moreover, it is concluded that the isolated cells in association with the new hydroxyapatite/silk fibroin composite proposed have had a beneficial effect on rabbits' skull defects healing.